Avec les compliments de Ph. Bernard

CERN/TC/BEAM 65-4
16.8.1965

THE CERN RF-SEPARATOR

H. Lengeler

This report describes the new CERN RF-separator that came into operation in January 1965. It is intended as a survey article for all those who are working with the RF separated beams, and has been written mainly because most of the ideas underlying this separator are spread throughout a large number of internal reports or unpublished notes.

The paper is divided into a theoretical part and a technical description of the apparatus. A final chapter is devoted to tolerances and particle losses.

THE CERN RF-SEPARATOR

I. THEORETICAL PART

1. Separation factors
2. Principle of operation
3. The RF separated beam
4. Energies of separation
5. The three-cavity system
6. Deflection structures
7. Acceptance - considerations
8. Comparison between electrostatic and RF-separators

II. TECHNICAL DESCRIPTION

1. The RF system
2. Trigger and timing system
3. The structure vacuum system
4. Interlock-systems
5. Phase reference system
6. Water cooling and power measurement system
7. The beam-stopper

III. TOLERANCES AND PARTICLE LOSSES ON THE BEAM-STOPPER

Appendix I Definitions and relations for electromagnetic fields in waveguides.

Appendix II Choice of deflecting waveguide dimensions.

PS/4999/dmh

THE CERN RF-SEPARATOR

I. THEORETICAL PART

Aiming at higher and higher energies of secondary beams, modern accelerator physics has reached the upper energy limit of electrostatic separators which lies at about 6 GeV for kaons and 12 GeV for antiprotons and pions. Therefore, in several high-energy laboratories there has been a search for devices enabling particle separation to be achieved up to much higher energies. We will not discuss in this paper the different solutions given to this problem [1] but concentrate on the CERN RF-separator built by a group of AR Division [2), 3), 4)] and based on a proposal made in 1959 by Panofsky at CERN (unpublished note).

1. Separation Factors

It is useful to look at the relative number of particles produced by high-energy protons impinging on a target. Taking a typical case of 10 GeV/c secondaries produced by 23 GeV/c protons in a Be-target, at 0^{o} production angle we obtain [5)]

$$\pi^- : K^- : \bar{p} = 308 : 11 : 1$$
$$p : \pi^+ : K^+ = 27 : 9.6 : 1$$

Decay of pions and kaons in a 180 m long beam transform these ratios to

$$\pi^- : K^- : \bar{p} = 220 : 1 : 1$$
$$p : \pi^+ : K^+ = 300 : 77 : 1$$

If these strongly interacting particles are used for taking bubble chamber photographs the number of unwanted particles should not exceed a few percent of the number of wanted particles. This requires separation factors η_s ranging from about 5000 - 10000

$$\left(\eta_s : \frac{\text{number of wanted particles at bubble chamber}}{\text{number of unwanted particles rejected by the separator}} \right)$$

A different problem is the contamination of such beams with muons produced by the decay of pions and kaons in the beam. Due to the small mass difference between pions and muons it is nearly impossible to separate the muons and pions at high energies by a "mass-spectrometer", but a careful design of the beam transport system can limit their number to a tolerable level. As muons are not strongly interacting particles their number can be near or even exceed the number of wanted particles although this makes scanning and reconstruction of events more difficult.

2. Principle of Operation

A continuous beam of particles of momentum p passes successively through two regions of RF-fields which exert a deflection force on the particles. The first one impresses onto the beam a high frequency structure which is analysed in the second field. The overall deflecting

force on the particles is dependent on their time of flight between the two fields and thus on their rest-mass, thereby enabling the separation of different kinds of particles to be obtained.

Before describing the operation of the separator in some detail, we note that the deflection is produced by a linearly polarised travelling wave (λ = 10.5 cm) supported by waveguides* similar to those used in linear electron accelerators. The RF-power needed to deflect high energy particles ($p > 10$ GeV/c) by an angle of about 1 mrad lies in the region of 10 - 20 MW. With current RF generators such high powers can only be achieved for pulse durations of some μsec. As the beam pulse passing through the separator must obviously be shorter than the RF pulse duration, only fast ejected beams of the CPS (having a pulse duration of 10 nsec to 2 μsec) can be used in conjunction with RF-separators.

These beam bursts are still long compared to the period of the RF-fields whose frequency lies around 3000 MHz.

Fig.1 illustrates the principle of operation of an RF-separator with two deflecting structures. A momentum analysed beam passes successively through two deflecting waveguides. The distance between the waveguides is large compared to their length. For simplicity we assume that the beam has negligible angular divergence. The relative phase of the RF-fields in the waveguides RF 1, RF 2 is kept constant and can be adjusted to any value. Midway between the two waveguides there is a beam-optical system which images the centre of RF 1 with unity magnification into the centre of RF 2.

Imagine a beam of kaons and pions of same momentum p passing RF 1 along the axis. The particles recieve a deflection $\varphi \sin\omega t$ depending on the field amplitude and on the entry phase ωt (φ : maximum deflection in one cavity, ω : angular frequency of RF-fields)

Behind RF 1 the beam has a fan-shaped form with half opening angle φ and is modulated in angle as $\sin \omega t$ (cf. Fig.1a where the trajectories of particles with different ωt are represented). If we make the cavities short enough the transit time difference of the two kinds of particles will be very small and the deflection is practically independent of the particle rest-mass. (This is in contrast to the electrostatic separator where spatial separation is achieved by the difference in transit time of two kinds of particles in a "long" electrostatic field)

The beam optical system transforms the deflections to $-\varphi \sin \omega t$. We adjust the relative phasing of RF 2 with respect to RF 1 in such a way that the entry phase of a pion (unwanted particle) is the same in RF 2 as in RF 1. Then it's second deflection will cancel the first one, provided the field-amplitudes in RF 1 and RF 2 are equal. All pions will then be brought back to the axis, independently of their entry phase ωt. In Fig.1b we have represented the case $\omega t = 90^{\circ}$.

* We often use the term "cavity" instead of waveguide or structure although we work with travelling waves.

A kaon, passing RF 1 at the same moment as a pion will arrive at RF 2 with a time delay corresponding to a phase difference τ because of it's greater rest-mass. It's final deflection will be

$$\varphi_w(t) = -\varphi \sin \omega t + \varphi \sin (\omega t + \tau)$$
$$= 2\varphi \sin \frac{\tau}{2} \cos (\omega t + \frac{\tau}{2}) \qquad (1)$$

The deflection of the kaon beam is thus modulated as sin ωt, the maximum value being $\varphi_w = 2\varphi \sin (\tau/2)$, and the kaons emerge from RF 2 again in a fan-shaped distribution. At some distance behind RF 2 there is a centrally placed beam-stopper whose thickness is chosen to intercept all pions (unwanted particles). It also intercepts some of the kaons (wanted particles) which are swept across it. However, if the peak deflection φ_w is big enough most of them will pass the beam-stopper and thereby spatial separation is achieved. The most favourable case is obtained for $\tau = 180^\circ$, then the deflection φ is just doubled in RF 2. (cf. Fig. 1b)

The accuracy of this time of flight method is given essentially by the frequency of the RF-fields, half a period corresponding to about 0.15 nsec.

If the beam opening $\pm \delta$ at the entry of RF 1 is not neglible, the maximum deflection of the wanted particles behind RF 2 is $\delta + 2\varphi$ whereas the divergence of the unwanted-particle-beam is again $\pm \delta$. The thickness of the beam-stopper has to be made corresponding at least to $\pm \delta$ in order to stop all unwanted particles. (cf. also I.7)

The loss of wanted particles on the beam-stopper could be avoided by using circularly polarized waves as originally proposed by Panofsky. Then the wanted particles are deflected on a conical surface of semi apex-angle 2φ, whereas the unwanted particles are brought back to the axis. A drawback of circular polarized waves is that two linearly polarized modes 90° out of phase must be excited thus requiring double RF power. Furthermore, with linearly polarized waves, the momentum analysis can be done in the horizontal plane and mass analysis in the vertical plane; this eases considerably the tolerances on lens aberrations and isochronism in the plane of momentum analysis.

3. The RF-separated beam

Fig.2 is a schematic layout of a RF-separated beam.[6] Secondaries are produced by a fast ejected beam and the acceptance of the beam is defined in the vertical and horizontal planes by two collimators followed by a momentum analyser in the horizontal plane.

This is very similar to an electrostatically separated beam, the only difference being the collimator C_5 (angle defining slit) which defines the angular interval in the vertical (mass separation) plane that is accepted by the RF-separator. (Unlike electrostatic separators which work with nearly parallel beams, the RF-separator can accept an angular interval of several mrad). After the momentum analysis the beam is focussed in both planes to the centre of RF 1. A symmetrical system of two doublets or one triplet

of quadrupoles then images the centre of RF 1 to the centre of RF 2 with unity magnification. Behind RF 2 the beam is again focussed and the unwanted particles are intercepted by a beam-stopper (which corresponds to the mass-slit in an electrostatically separated beam) whereas the wanted particles pass on either side. They enter a second momentum analyser which is intended mainly to reduce the μ-contamination. Finally a beam-shaping optical system makes the beam nearly parallel in the vertical plane and brings the particles to the Bubble chamber.

In order to reduce the μ-background the phase space occupied by the beam is several times rigorously defined. This explains the large number of collimators used in the beam.

We note that the vertical acceptance of the beam before the separation stage is about 3 times smaller than the horizontal acceptance, since the former must allow for the increase in angle that occurs for the wanted particles behind RF 2 in the vertical plane.

4. Energies of Separation

In calculating the energies of separation we have to distinguish between separation of one kind of wanted particle from one or two kinds of unwanted particles.

Inspection of the particle ratios quoted in 1., shows that in general two kinds of particles have to be rejected, but in the case of π^+ separation at 10 GeV/c for example, it is sufficient to reject only the p because the number of K^+ is about 80 times smaller than the number of π^+.

In the following we characterize unwanted particles by subscripts a, b, and wanted particles by a subscript w.

a) Single Particle Rejection

By proper choice of the phase between RF 1 and RF 2 the final deflection of unwanted particles can be made zero at all times, whilst the maximum deflection of the wanted particles is given by

$$\Psi_w = 2\varphi \sin \frac{\tau_{aw}}{2} \qquad (2)$$

τ_{aw} being the phase shift between the two kinds of particles over the distance L between RF 1 and RF 2.

τ_{aw} can be calculated for two relativistic particles a, w of momentum p using the formula

$$\tau_{aw} = \frac{\pi L f}{2c} \frac{(M_a^2 - M_w^2)\, c^4}{p^2 c^2} \qquad (3)$$

M_a, M_w : rest-masses

$f = \frac{\omega}{2\pi}$: frequency of RF fields (2855 MHz)

$pc >> M_a c^2, M_b c^2$

This shows that separation of one kind of particle from one other kind is possible for a continuous momentum range, except for those momenta where $\tau_{aw} = 2N\pi$, $N = 1, 2, \ldots$ The highest value of φ_w is obtained for $\tau_{aw} = (2N-1)\pi$. We call "design-momentum" p_o the momenta given by the condition $\tau_{aw} = \pi$.

In Table 1a we have listed the separation momenta corresponding to $\tau_{aw} = \pi, 3\pi$, and some related quantities.

b) Two Particle Rejection

If two kinds of unwanted particles a, b have to be separated from a third one w, the final deflection of the most abundant particle, say a, can always be made zero by choosing the right phase between RF 1 and RF 2. The final deflection of particles b can also be made zero if the condition holds

$$\tau_{ab} = 2N\pi \qquad N = 1, 2, \ldots \qquad (4a)$$

For the wanted particles we obtain again

$$\varphi_w = 2\varphi \sin \frac{\tau_{aw}}{2}$$

which is maximum for

$$\tau_{aw} = (2N - 1)\pi \qquad (4b)$$

As we will see later, the most important condition is (4a) because deviations from (4a) influence strongly the width of the beam of unwanted particles.

Obviously (4a) can only be fulfilled for some well-defined momenta. Thus, in contrast to the one particle rejection, two particle rejection is not possible in a continuous momentum interval, (using only 2 cavities).

The design momentum of the CERN RF-separator (for $K^{\pm}$) is $p_o = 10.32$ GeV/c ($\tau_{\pi K} = 180^o$) and was chosen sufficiently above the practical limit for $K^{\pm}$ separation with electrostatic separators.

The upper limit of the useful momentum band is given by the flight-path length, the available RF power and the beam transport system handling momenta up to 20 GeV/c. The lower limit is determined by anisochronism due to finite momentum bite and also by μ-contamination, it lies around 7 GeV/c.

The available flight-path length in the East Area of CPS is up to 50 m. It can be made smaller, but for beam optical reasons the lower limit is about 20 m.

In Table 1b we have listed the separation momenta and some related quantities for two-particle rejection and for three values of L.

We do not consider higher values of τ_{ab} than 2π and 4π because phase stability tolerances become impractically tight.

The case of $\bar{p}$ -separation above 12 GeV/c needs special attention. The phase difference between π^- and K^- becomes much smaller than 2π at these momenta. One therefore tries to cancel exactly the deflections of the π^- and has then to deal with a non-zero deflection of the K^- : $\varphi_K = 2\varphi \sin \frac{\tau_{\pi K}}{2}$.

To stop all K^-, one has to increase notably the beam-stopper thickness, at the same time increasing considerably the losses of $\bar{p}$ on the beam-stopper. In Section III we give an analysis of these losses.

TABLE 1a

Length	Momentum GeV/c.	τ_{aw}	$\left\|\sin \frac{\tau_{aw}}{2}\right\|$	$\left\|\sin \frac{\tau_{ab}}{2}\right\|$
	π^+ Separation		p Rejection only	
		$\tau_{\pi p}$	$\left\|\sin \frac{\tau_{\pi p}}{2}\right\|$	$\left\|\sin \frac{\tau_{pK}}{2}\right\|$
50 m	20.5	180°	1	0.928
	11.7	540°	1	0.320
28 m	15.1	180°	1	0.920
	8.72	540°	1	0.375
22 m	13.4	180°	1	0.920
	7.75	540°	1	0.370

Length	π^- Separation Momentum GeV/c.	$\tau_{\pi K}$	K^- Rejection only $\left\|\sin \frac{\tau_{\pi K}}{2}\right\|$	$\left\|\sin \frac{\tau_{Kp}}{2}\right\|$
50 m	10.32	180°	1	0.970
28 m	7.72	180°	1	0.970
22 m	6.85	180°	1	0.970

TABLE 1b

Length	Momentum GeV/c.	$\sin\frac{\tau_{aw}}{2}$	τ_{ab}	$\sin\frac{\tau_{ab}}{2}$
	K^- Separation		(π^-, $\bar{p}$ Rejection)	
		$\left\lvert\sin\frac{\tau_{Kp}}{2}\right\rvert$	$\tau_{\pi p}$	$\sin\frac{\tau_{\pi p}}{2}$
50 m	14.3	0.73	360°	0
	10.10	0.997	720°	0
28 m	10.7	0.72	360°	0
	7.56	0.99	720°	0
22 m	9.47	0.71	360°	0
	6.7	0.99	720°	0
	π^- Separation		(K^-, $\bar{p}$ Rejection)	
		$\left\lvert\sin\frac{\tau_{\pi K}}{2}\right\rvert$	τ_{Kp}	$\sin\frac{\tau_{Kp}}{2}$
50 m	12.3	0.895	360°	0
	8.7	0.78	720°	0
28 m	9.2	0.85	360°	0
22 m	8.15	0.9	360°	0
	p ($\bar{p}$) Separation		(K, π Rejection)	
		$\left\lvert\sin\frac{\tau_{pK}}{2}\right\rvert$	$\tau_{K\pi}$	$\sin\frac{\tau_{K\pi}}{2}$
50 m	7.30	0.445	360°	0
	$\bar{p}$ Separation with $\sin\frac{\tau_{ab}}{2} \neq 0$			
		$\left\lvert\sin\frac{\tau_{p\pi}}{2}\right\rvert$	$\tau_{K\pi}$	$\left\lvert\sin\frac{\tau_{K\pi}}{2}\right\rvert$
50 m	18	0.915	59.3°	0.495
	20	0.999	48.1°	0.407
28 m	20	0.784	26.9°	0.233
	18	0.897	33.2°	0.286
	14	0.964	54.9°	0.461
22 m	20	0.65	21°	0.182
	15	0.95	37.5°	0.320
	12	0.92	58.5°	0.448

5. The Three-Cavity System

The two-cavity system described has an important drawback: it is not possible to separate two kinds of unwanted particles from a third one in a continuous momentum interval.

This difficulty can be overcome by a three-cavity system proposed by Sehnell [7].

There are three identical cavities separated by drift spaces L_1 and L_2 and by lens systems like the ones described above. One can show that by energizing simultaneously the three cavities amplitudes and relative phases can be adjusted in such a way that the final deflections for both unwanted particles are zero. Generally the deflection of the wanted particles is then different from zero. We will not go into the details of this device which will be subject of further work.

As one will not give up the possibility of separating particles by energizing only two out of three cavities the distances L_1 and L_2 should be different. Recalling that $L_1 + L_2 \approx 50$ m and L_1, $L_2 \geqslant 20$ m a reasonable choice is $L_1 \approx 20$ m, $L_2 \approx 30$ m.

6. Deflecting structures

For the operation of a Panofsky-type RF-Separator we need structures that can support high-frequency fields with deflecting properties.

We first estimate at which frequency we should work. At an energy of 10 GeV/c the time delay of π, K and p with same momentum over 50 m flight path is some tenths of a nsec. This has to correspond to a few periods of the high frequency fields used, thus giving frequencies in the GHz-regions.

Cavities or waveguides supporting RF fields must have transverse dimensions of the order of the free space wavelengths involved. To make the openings not too small, the wavelengths should not be smaller than a few cm.

As the high-frequency powers needed are in the range of many MW we have to look for H.F. generators of this power range. A suitable choice seemed to be S-band frequencies ($\lambda \approx 10$ cm), because there are 20 MW Klystrons available. The final choice of frequency was around f = 2855 MHz (λ = 10.5 cm).

To support the H.F.fields one can use either cavities in a standing wave mode or waveguides in standing or travelling wave modes. In a single standing wave cavity the deflection of particles is dependent on a transit time factor, thus one is limited in length and thereby in deflecting angle. This is rather serious for particles of many GeV/c. One can overcome this by a series of cavities coupled together but the problem of correct phasing being tedious, one is lead to waveguides with travelling wave-modes. Waveguides can be operated in standing-wave mode but peak electrical fields are doubled, increasing highly the danger of electrical breakdowns.

Clearly the interaction between particles and travelling waves will be highest if the particle velocity v equals the phase velocity v_φ of the wave. For the momentum range, where the separator is expected to work ($\sim$10 GeV/c) we have $v \approx c$.

One can show [8] that the deflection force for a particle in synchronism with a wave is equal to

$$F_T = \frac{e}{2\pi} \lambda \, \mathrm{grad}_T E_z \qquad (5)$$

e : charge
λ : free space wavelength of the field.

From (5) one concludes that for TE-modes where $E_z \equiv 0$, the electrical forces are compensated exactly by the magnetic forces. This is valid for all v_φ.

For TM-modes the deflection force is proportional to $1 - \frac{v_\varphi^2}{c^2}$, and becomes very small for highly relativistic particles. Thus neither TE nor TM-modes are suited for the deflection of highly relativistic particles.

B.W.Montague [9] at CERN, following a suggestion of Walkinshaw showed that there exist other types of deflecting modes, called hybrid modes, whose deflection forces do not tend to zero for $v_\varphi \longrightarrow c$.

These modes have been extensively studied in several laboratories [8]- [12] and it was shown that -

1) Hybrid modes form a set of independent solutions of Maxwell's equation, having in general longitudinal and transversal E and H components (hence the nomenclature EH-modes adopted by Garault [8] which we follow).
2) One can consider these modes as a mixture of E and H modes (name!)
3) Unlike E and H modes they do not lose their deflection properties at $v_\varphi = c$.
4) The simplest modes have deflection properties and are those of order 1 (with dipole symmetry). Higher order modes have quadrupole, sextupole... etc. symmetry and corresponding properties.
5) Hybrid modes do not fulfill boundary conditions in smooth waveguides but they can be supported by iris-loaded waveguides. (Fig. 3)

The exact field distribution in an iris-loaded guide cannot be expressed in closed form and it is therefore customary to develope the solution in the form of an infinite series, as is done for linac structures.

However one can get a very good knowledge of the field properties in calculating them in a simple approximation, the so-called "small pitch" approximation. One obtains it by supposing that there is an infinite number of infinitely thin irises loading the waveguide. This permits neglecting all space harmonies not corresponding to the principal deflecting mode $(EH)_{11}$ and one obtains for the field components [9] in a cylindrical

waveguide at $v_\varphi = c$

$$\left.\begin{aligned} E_r &= E_o\left[\left(\frac{kr}{2}\right)^2 + \left(\frac{ka}{2}\right)^2\right]\cos\theta \\ E_\theta &= E_o\left[\left(\frac{kr}{2}\right)^2 - \left(\frac{ka}{2}\right)^2\right]\sin\theta \\ E_z &= E_o.kr.\cos\theta \\ Z_o H_r &= -E_o\left[\left(\frac{kr}{2}\right)^2 - \left(\frac{ka}{2}\right)^2 + 1\right]\sin\theta \\ Z_o H_\theta &= -E_o\left[\left(\frac{kr}{2}\right)^2 + \left(\frac{ka}{2}\right)^2 - 1\right]\cos\theta \\ Z_o H_z &= -E_o.kr.\sin\theta \end{aligned}\right\} \qquad (6)$$

where E_o = maximum deflecting field strength

Z_o = wave impedance of free space

$k = \frac{2\pi}{\lambda}$ (free space propagation constant)

a = inner radius of waveguide irises

One can easily show that the force acting on a particle travelling parallel to the z-axis and in synchronism with the wave is given by

$$\left.\begin{aligned} F_r &= E_o \sin\theta \\ F_\theta &= E_o \cos\theta \end{aligned}\right\} \qquad (7)$$

The deflection force thus does not vanish and is of the order of E_o. Furthermore (7) shows that it is uniform over the cross-section and thus free of aberration, a very important property for a separator.

The force is linearly polarised in the $\theta = \frac{\pi}{2}$ direction and has no accelerating effect on the particles travelling along the axis.

Finally, one can look at the energy flux P, it is given by

$$P = \frac{-2\pi E_o^2}{k^2 Z_o}\left[\left(\frac{ka}{2}\right)^4 - \frac{4}{3}\left(\frac{ka}{2}\right)^2\right] \qquad (8)$$

For given k the sign of P is fixed by the inner radius a because for

$ka = \sqrt{3}$ $\quad P = 0$ (zero group velocity)

$ka > \sqrt{3}$ $\quad P > 0$ (forward wave)

$ka < \sqrt{3}$ $\quad P < 0$ (backward wave)

The actual waveguide supporting hybrid modes cannot have infinitly small pitch but is loaded with irises of finite thickness and spacing (Fig.3) and with rounded edges.

The central fields now penetrate in the loading region and one must introduce space harmonics to match the boundary conditions. This was done by a computer programme [13], [14].

In close conjunction with the computer studies, extensive model measurements [11] were made to determine the dimensions of an iris-loaded waveguide suitable to support at 2855 MHz a deflecting hybrid mode with $v_\varphi = c$.

In Appendix II, we give a short discussion of the waveguide parameters finally adopted.

It turns out that the dimensions a and the ratio d/D (cf. Fig 3) are already fairly well determined by the small-pitch approximation. The same applies to the dispersion curve of the waveguide. (Fig.12). As the higher harmonics introduced in the computation have widely different phase velocity from the fundamental mode, they do not affect the deflection force. Hence, the uniformity of force over the cross-section is not affected.

In Fig. 4 we have represented a somewhat detailed sketch of the actual field configuration in the loaded waveguide [8]. One notes two flats that fix the plane of polarisation of the deflecting wave.

In Table 2 some structure parameters are listed together (cf.Appendix II)

(Table 2 overleaf)

7. Acceptance Considerations

As each deflecting structure has a length of 3 m and an inner diameter of 55 mm., the acceptance of the structure is limited and we must try to exploit it to the maximum. One way of doing this is to put a beam focus in the centre of RF 1 and to image this focus by a lens system in the centre of RF 2. This can be conveniently done by putting midway between RF 1 and RF 2 a symmetrical quadrupole triplet (or two doublets) whose transfer matrix is given by

$$\begin{pmatrix} -1 & 0 \\ \alpha & -1 \end{pmatrix} \qquad (9)$$

α can be different for the two planes. In the vertical (mass separation) plane we put $\alpha = 0$ obtaining by this a complete 1 : 1 imaging which gives cancellation of possible aberrations in the RF deflection structures.

There is another advantage of the 1 : 1 imaging. B.W.Montague [15] has shown that the effect of a cavity of finite length is equivalent to a deflection plus a displacement occurring at the centre of the cavity. If we assume that the deflecting wave has constant amplitude and velocity throughout

Table 2

Separator and structure parameters

Design momentum p_o (K - π)	10,32 GeV/c
" " p_o (p - π)	20,5 GeV/c
Cavity spacing L	20 - 50 m
RF-pulse length	8 μsec
repetition rate	~ 1 pulse/sec
peak power per cavity	20 MW
peak transverse momentum	~ 17 MeV/c
frequency f	2854,75 MHz
wave length $\lambda = \lambda_g$	10,5 cm.
cavity length ℓ	3 m.
cavity half aperture	2,75 mm.
cavity acceptance (vertical)	4,20 mm mrad
" " (horizontal)	4,60 mm mrad
number of cells/structure	114
number of cells/wavelength	4
phase shift per cell	$\frac{\pi}{2}$
v_g/c	0,0189
dispersion D	52
filling time	0,53 μsec
v_φ/c	1
Q-value (measured)	~ 9500
Voltage attenuation coefficient	0,17 Neper/m

PS/4999/dmh

the structure the effective peak deflection φ_ℓ and the peak displacement x are given by

$$\varphi_\ell = \varphi \frac{\sin \tau_\ell/2}{\tau_\ell/2} \qquad (10)$$

$$x = \frac{\varphi_\ell}{2} \frac{1}{\tau_\ell} \left(\cos \frac{\tau_\ell}{2} - \frac{\sin \tau_\ell/2}{\tau_\ell/2} \right) \qquad (11)$$

where τ_ℓ is the phase shift between particle and wave over the cavity length ℓ and φ the maximum deflection for a particle with $\tau = \tau_\varphi$. One will try to make $\tau_\ell = 0$ for the particles because this gives $\varphi_\ell = \varphi$ and $x = 0$. If, however, $\tau_\ell \neq 0$ particles undergo a reduced deflection and a finite displacement. Both effects will be exactly cancelled if we use a 1 : 1 imaging system between RF 1 and RF 2.

Having fixed the lens system between the two cavities we look now for optimum acceptance conditions. This can be conveniently done by considering the phase plane of mass separation.

Fig. 5 shows the phase plane diagram in the centre of the first cavity. Transformation of the output and input aperture limits gives two pairs of limiting lines inside which the beam must remain. (We assume that acceptance is limited by the square inscribed in the circular iris section).

The incoming beam (angular opening 2δ) is shaped by collimators and a quadrupole doublet to occupy a rectangle with one side parallel to the x-axis*.

This is done by imaging the target (or C_4) by a lens doublet in the centre of RF 1 and by putting the "angle defining" slit (C_5) at the focus of the same doublet, thus imaging it to infinity (cf. Fig. 2)

After deflection in RF 1 the beam occupies a rectangle corresponding to a beam opening $2(\delta + \varphi)$ the particles being spread over this area independently of their rest mass. This configuration is transformed by the matrix (9) without changing its form. The deflection in RF 2 cancels the deflection of unwanted particles; they are brought back to a rectangle with opening 2δ. The deflection of the wanted particles is increased to $\psi_w = 2\varphi \sin (\tau_{aw}/2)$; they occupy now a rectangle with opening $2(\delta + \psi_w)$.

The beam is then projected by another lens system on a beam-stopper whose thickness is adjusted, just to stop all unwanted particles. If one transforms the beam-stopper back to RF 1 it just covers the area occupied by the unwanted particles.

Obviously maximum acceptance is reached if the beam half-width d is:

$$d = X \text{ max}/2 \qquad (12)$$

---

* One can imagine unsymmetrical beam-shapes that give higher acceptance. As they are not used in the new U_1 beam we don't discuss them here, (cf. Montague [16]).

and if $\delta + \psi_w = X'max/2$ with $\psi_w = 2\varphi \sin \frac{\tau_{aw}}{2}$

Maximising of the flux of wanted particles passing the beam-stopper gives another relationship between δ and ψ_w

$$\psi_w = 2\delta \tag{13}$$

Optimum conditions are thus obtained if the beam half opening is

$$\delta = \frac{X'max}{3} \tag{14}$$

and if the maximum deflection in both cavities is

$$\varphi = \frac{\delta}{\sin \frac{\tau_{aw}}{2}} \tag{15}$$

8. Comparison between Electrostatic and RF-Separators

For an electrostatic separator the difference in deflection angle for two particles of different rest masses m_1, m_2 and momentum p is given by

$$\Delta\varphi_s = \frac{eE\ell}{pc} \Delta\left(\frac{1}{\beta}\right) \tag{16}$$

e : charge of particle; E : electrostatic field strength; ℓ : length of separator.

$$\Delta\left(\frac{1}{\beta}\right) = \frac{1}{\beta_1} - \frac{1}{\beta_2}$$

for ultra-relativistic particles this can be written

$$\Delta\varphi_s = \frac{eE\ell}{2(pc)^3} (m_1^2 - m_2^2) c^4 \tag{17}$$

For the RF separator we get instead for the deflection angle of unwanted particles zero and for the wanted particles

$$\psi_w = \frac{2e\bar{E}\ell}{pc} \sin \frac{\tau_{aw}}{2} \tag{18}$$

where $\bar{E}$ is an "equivalent" electrical field strength that can be made at least as high as E in the electrostatic case.

For design momentum we have

$$\sin \frac{\tau_{aw}}{2} = 1$$

Comparison of (17) and (18) shows that the small term $\Delta(1/\beta)$ which gives rise to a $1/p^3$ law is absent in the RF-separator case (near design momentum!)

It is mainly this $1/p^3$ law that limits the electrostatic particle separation at high energies.

From (16) and (18) one can deduce that for e.s. separators the separation is determined by a difference in deflection angle and is proportional to the difference in time of flight of the two particles over the separator length ℓ, whereas for the RF-separator the separation is determined by the deflection angle of wanted particles and dependent on the time of flight over the cavity length itself.

If we do not work with the RF-separator under optimum condition, i.e. near design momentum p_o, we can introduce the p-dependence of τ_{aw} and obtain with $\tau_{aw} \propto 1/p^2$

$$\sin \frac{\tau_{aw}}{2} = \sin \left[\left(\frac{p_o}{p} \right)^2 \frac{\pi}{2} \right] \qquad (19)$$

thus introducing (19) in (15)

$$\gamma'_w = \frac{2eE\ell}{pc} \sin \left[\left(\frac{p_o}{p} \right)^2 \frac{\pi}{2} \right]$$

for $p \gg p_o$ this can be written

$$\gamma'_w = \frac{2eE\ell}{pc} \left(\frac{p_o}{p} \right)^2 \frac{\pi}{2}$$

The design momentum p_o is given by the condition $\tau_{aw} = \pi$, thus

$$\gamma'_w \approx \frac{eE\ell}{2(pc)^3} (m_a^2 - m_w^2) \left(\frac{2\pi L}{\lambda} \right) \qquad (20)$$

Thus in this case the deflection shows as in the e.s. deflection case, a $1/p^3$ behaviour, but comparison of (20) and (17) shows that in the RF-deflection formula there is an additional factor $\left(\frac{2\pi L}{\lambda} \right)$ which, using microwaves, can be made very big. In our case its value is about 3000.

A drawback of the present RF-separator is it's small pulse duration. Due to the high microwave power needed (about 10-20 MW) the pulse length can only be made a few μsec. Therefore, the RF-separator is interesting mainly for Bubble Chamber physics. The short pulse length also implies that it must work with a fast-ejection system of the P.S.

Currently there are superconducting RF cavities [17),18),19)] in different laboratories under study, making possible much longer RF-pulses. This could extend the field of application to counter physics and to energy regions above 100 GeV/c.[20)]

II. TECHNICAL DESCRIPTION

1. The RF System

In Fig. 6 we have represented a functional diagram of the RF system of one RF-separator station.

a) The Klystron and its HT-Modulator

The heart of this layout is a 20 MW-klystron amplifier (Thomson-Houston 2011 C) with four cavities. The internal electron-beam is focused by coils surrounding the cavities. An active getter ensures sufficiently good vacuum inside the klystron. The high tension for the klystron is supplied as a 240 kV negative, 8 μsec pulse to the cathode. It is produced by a pulse forming network (delay line) feeding into a pulse transformer and discharged by a triggered spark switch.

In its present form the charging circuit of the delay line produces one pulse per second. It could, however, be changed to give a train of several pulses with some millisecond spacing, useful in multi-expansion operation of the 200 HBC.

The high tension is stabilized to some 0.2 % by a magnetic amplifier system.

The HT circuit is protected against over-voltage by an additional safety spark gap followed by an interlock system to switch off the HT charging circuit. A similar interlock system protects the charging circuit against over-current.

The lower part of the klystron. the charging circuit, delay line, pulse transformer and the heater supply are immersed in an oil tank.

The HT Modulator and its control system were built by Vickers Research Ltd., (England).

b) The RF-Generator Chain [21]

RF is generated at a frequency of ~2855 MHz with a C.W.-Pound-klystron generator stabilized by an invar cavity to $\Delta f/f \approx 3.10^{-6}$.

This signal is amplified in a two stage modulated klystron amplifier which supplies a 10 kW RF-pulse of variable length (6 - 12 μsec).

The output is fed through a three-way power divider and a 30 m. HF cable (drive cable) into the 20 MW klystron.

A variable attenuator enables the klystron to be run with saturated input so that output power is substantially independent of input power.

A phase shifter in the drive line (which forms part of the phase system described below) permits changing the relative phase between the two cavities of the separator. Frequency can be measured and monitored by a high precision wavemeter.

c) The High Power Chain

The amplified RF power is taken out from the klystron by two waveguide channels and afterwards recombined in a hybrid transformer (circular magic-tee). A remote controlled phase shifter makes it possible to change the distribution of power between the cavity and a 10 MW matched load, thus enabling amplitude changes to be made in the cavity without touching the HT applied to the klystron. This is desirable because the klystron should be operated at maximum power level where its phase stability is best. The waveguide system between klystron and cavity is pressurized to about 3 atm. (air) to minimize the risk of RF breakdown. Separation of this pressurized part from the klystron and from the cavity which are both under high vacuum is ensured by ceramic windows. The output end of the cavity is closed by a matched water load where the absorbed power can be measured.

2. The Trigger and Timing System

The drive chain and the HT spark gap are triggered by a "Master trigger generator" that can operate with an internal time base of 1 or 10 pulses/sec or with an external timing unit [22].

As the klystron modulator should work at a repetition rate of about 1 pulse/sec and as the PS cycle is generally longer (2 - 5 sec) this timing unit has two functions.

1) It must produce a trigger pulse related to a PS pulse (or more exactly to a pulse triggering the fast ejection kicker) in synchronism with the beam passing the separator.

2) It must produce "fill-in" pulses between the PS pulses of about 1 second time interval.

It also supplies gate pulses for the different counters used in the RF separated beam.

3. The Structure Vacuum System (Fig. 7)

Each structure is made up of 3 sections of iris-loaded waveguide supported on a rigid girder to prevent mechanical deformation. Facilities for lining up the structure in a beam and for taking it out rapidly are foreseen.

To avoid as much as possible breakdowns due to high electrical fields, each cavity is evacuated to about 10^{-8} Torr by cold-cathode ion pumps. Outgassing is reduced by using mainly metallic joints (indium or gold) or baked-out Viton joints. The initial pumping-down to around 10^{-4} Torr is made by a Roots-pump backed by a rotary pump.

Isolation from rough vacuum in the beam tubes is provided by 6 micron thick mylar-windows that withstand 1/3 of an atm. Two 90° degree valves make it possible to isolate completely the cavities from the beam transport system without affecting the high vacuum. During runs these valves are opened to give free passage to the beam.

An interlock system closes them automatically if the pressure in the beam tubes rises above 10^{-1} Torr. At the same time a by-pass valve opens equalizing pressure on both sides of the mylar-window.

Rough vacuum at both ends is measured by thermocouples, high vacuum inside by an ionization gauge that can be set to switch off at a given maximum pressure. It is combined with an interlock system that switches off at the same time the klystron HT, thus protecting the system against electrical breakdown inside the structure, caused by bad vacuum.

4. Interlock Systems

Besides the vacuum interlock system, protection against electrical breakdown in the pressurized waveguide system is ensured by photodiodes looking at the ceramic window that isolates the pressurized part from the structure. As breakdowns are generally accompanied by a visible glow of light on these windows, the output of photodiodes can be fed to the interlock system that switches off klystron HT. This protects the ceramic windows of the klystron against overheating by repeated electrical breakdowns.

Several pick-up probes are installed on the input and output side of the structure to detect a lack of RF pulses. This occurs if there is an electrical breakdown or if HT and/or RF input signal is missing. Their output is fed into a veto system that prevents the Bubble Chamber flashes from being triggered if RF pulses are missing or if they are deformed.

Some other interlocks protect the system against water failure (cooling of klystron anode and focus coils) and compressed air failure (pressurized waveguides and spark switch).

5. Phase Reference System [23]

As the operation of an RF separator requires a phase stability between the cavities of a few degrees, changes of phase during operation should be corrected.

The RF system (Fig. 8) is made up of a common RF generator whose output signal is fed via a transmission cable (drive cable) to the 20 MW klystron. A waveguide system connects the klystron with the structure.

The relative phase of two cavities can be held constant by picking up signals from the two cavities (actually from the input couplers) and comparing them in a phase bridge whose output is used to adjust a phase shifter in the drive line of one of the klystrons.

Such a system cannot correct phase errors within one RF pulse (8 μsec long), but will correct slow phase drifts. The main causes of such slow phase drifts are temperature changes in the drive transmission line and in the waveguides, frequency changes of the generator and changes in klystron high tension.

The phase comparison circuit (phase reference) involves a transmission line, connecting the two cavities of about 60 m length ($\sim$ 600 wavelengths).

If we need a phase stability better than 2°, the relative phase constancy in the reference phase cable must be better than one part in 10^5 and can only be achieved by temperature stabilizing. We use a helical-membrane cable (UR79) which is essentially air spaced ($v_\varphi/c = 0.96$). Phase changes are then due mainly to changes in length of the inner and outer conductors with temperature and to changes of dielectric constant of air with pressure. The temperature-stabilizing system keeps T constant to a few tenths of a degree by means of a sampling circuit which uses the outer Al-conductor as both heating and temperature sensing element. The outer conductor of the drive cable is used as a return conductor.

The phase bridge is placed midway between RF 1 and RF 2 so that the phase changes due to air pressure variations are nearly cancelled.

In one of the phase reference cables there is a remote controlled phase shifter (reference phase-shifter) that can be set to any value between 0° - 360° and allows any wanted phase setting between the two cavities.

The phase bridge is a coaxial-line hybrid ring having in its two output channels crystal detectors. The mean rectified signal can be made independent of field amplitudes in the cavities. It is amplified, gated so as to use only the middle part of the RF-pulse which is independent of built-up effects in the cavities, and fed into a pulse-lengthener whose output voltage is proportional to the phase deviation from the chosen reference phase.

This pulse-lengthener feeds a small DC motor which adjusts the position of the (drive) phase shifter in the drive transmission line until the correct phase between RF 1 and RF 2 is established.

We note the importance of a high phase stability in the phase reference cable. Any phase error in the reference system is automatically corrected by a corresponding phase shift in the drive system, thus giving an error in the relative phase of RF 1 and RF 2.

6. Water Cooling System and Power Measurement System [24]

Due to its high dispersion the RF structure used has a large temperature dependence of frequency (-50 kHz/$^{\circ}$C) and it is important to hold the temperature of the disc-loaded waveguides at constant and uniform temperature.

At a repetition rate of 1 pulse/sec, 20 MW input power and 8 μsec pulse length, the mean power deposited in the structure and in the matched load is only 160 Watt. Therefore, the cooling does not present a problem and is done by a water jacket surrounding the structure. This water is held at constant temperature by a thermostat with cooling loops. (Fig. 9)

Small differences of the frequencies corresponding to $v_\varphi = c$ in the different structures due to small dimensional differences can be corrected by different water temperatures.

The power measurement is done with a matched water load at the output end of the structure. One measures the increase in temperature of water flowing

through a quartz pipe inside the load. This is done by temperature dependent resistors and conventional bridge techniques. As there is some heat loss through the walls of every load and it is difficult to reduce this, we made it constant and independent of outer temperature by surrounding each load by a water jacket held at the same temperature as the structure. Each load was calibrated by dc-heating of the water inside the quartz tube at a known flow rate.

We get a constant flow rate by using a volumetric pump of membrane-type that is triggered by a P.S. pulse. Therefore, we are independent of the repetition rate used.

The bridge output is fed into a magnetic amplifier and then recorded continuously on a recorder. The whole system has an accuracy of some percent.

The water is continuously deionized and there is a water flow indicator combined with an interlock system protecting the measuring system against water failure.

7. The Beam-stopper [25]

The beam-stopper is made of two wedge-shaped brass plates of 1 m length which can be moved parallel or anti-parallel against each other by remote controlled motors (see Fig. 10). The thickness T can be adjusted between 0 and 40 mm. as well as the height relative to the beam (at least $\pm$ 5 mm.). At maximum opening the stopper clears completely the beam tube. A high energy particle traversing the brass plates will suffer an energy loss by ionization of about 1.5 GeV/c. This is more than enough to remove it from the beam in the momentum analyser following the beam-stopper.

To enable an easy centering and monitoring of the stopper two scintillator counters of 10 mm thickness are fixed at the end of the two brass plates. They thus count particles that do not hit the beam stopper. The stopper is placed inside a dural-box that can be fixed to the beam tubes and evacuated.

III. TOLERANCES AND PARTICLE LOSSES ON THE BEAM-STOPPER

We remember the phase space considerations of chapter I, 7, where we found that the beam-stopper thickness had to be made to correspond exactly to the beam opening 2δ in the centre of RF 1. In this case it intercepts all unwanted particles provided the final deflection of unwanted particles can be made equal to zero. Every departure from this exact cancellation blows up the beam of unwanted particles and makes necessary, therefore, an increase in beam-stopper thickness. As we will see below, this increases the losses of wanted particles. For the wanted particles fluctuations in the final deflection are harmless because they are anyway spread over the total phase space available to them.

Cancellation of deflection of unwanted particles can be affected by:

a) errors in the phasing system between RF 1 and RF 2.

b) field-amplitude fluctuations in RF 1 and RF 2.

c) errors due to a phase-slip between particles and waves.

d) aberrations in the cavities.

e) anisochronism due to lens aberrations and finite beam openings.

f) errors due to finite momentum bite.

Let us discuss first in some detail these errors and then discuss how they must be combined to find the increase in beam-stopper thickness.

a) Errors in the Phasing System

1) These can be due to frequency fluctuations Δf during one RF pulse, changing the wavelengths in the drive cable and waveguides between RF generator and structure. The length of these cables and waveguides is around 300 wavelengths; we get for the phase change $\Delta\tau(f)$

$$\frac{\Delta\tau(f)}{2\pi} = 300\,\frac{\Delta\lambda}{\lambda} = 300\,\frac{\Delta f}{f}$$

Our RF generator has a stability $\Delta f/f = 3.10^{-6}$

thus $\Delta\tau = 0.32^{\circ}$

2) Ripples on the HT-pulse applied to the klystron affect the velocity of the internal electron beam and therefore the phase.

For the klystron chosen, it is about $8^{\circ}/kV$, we can reduce the phase error due to ripples to less than $\pm 2^{\circ}$.

3) Errors in the reference system controlling the relative phase between RF 1 and RF 2 can be due to inaccuracies in the feedback loop or to temperature effects in the phase cables between structures and phase bridge. They can probably be made smaller than $\pm 2^{\circ}$.

Adding these errors as statistically independent we get for the total error in the phasing system $\Delta\tau\,(\mathrm{Ph}) \approx \pm 3^{\circ}$.

b) Field-amplitude Fluctuations in the Cavities

The power input P_0 to the cavities can be controlled to better than $\pm$ 5 % accuracy. As $P_0 \alpha \varphi^2$ (φ : maximum deflection in one cavity) this corresponds to deflection fluctuations of $\pm$ 2.5 %.

c) Errors due to a Phase Slip between Wave and Particle

If the phase velocity of the wave inside the cavities is different from the particle velocity, there occurs a phase slip τ_ℓ over the length ℓ between particle and wave, and the deflection is reduced by a factor $\frac{\sin \tau_\ell/2}{\tau_\ell/2}$ (cf.(10))

As there is a symmetric 1 : 1 lens system between RF 1 and RF 2, this effect cancels exactly if it occurs in the same way in both cavities.

It is nevertheless worthwhile to look at the values for τ_ℓ because they cause a reduction in deflection that should obviously not be too big.

We first consider phase slips due to $v_\varphi \neq c$. v_φ can be changed mainly by frequency changes and temperature changes in the waveguides.

1) Frequency changes

In a waveguide with dispersion $D = \frac{c}{v_g} - 1$ we get (cf. Appendix I)

$$dv_\varphi / v_\varphi = -D \frac{df}{f} \qquad (21)$$

The phase slip between a particle with velocity c and the wave is given by

$$\tau_\ell = 2\pi . D . n . \frac{\Delta f}{f} \qquad (22)$$

where n is the number of wavelengths of the structure.

We have $n = 29$, $D = 52$, $\Delta f / f < 3.10^{-6}$

thus $\tau_\ell < 1.6^{\circ}$

The reduction in amplitude corresponding to this is negligible.

2) Temperature changes

For our structure we get $\frac{\Delta f}{\Delta T} = \frac{-50\,\mathrm{kHz}}{^{\circ}\mathrm{C}}$ (23)

As a temperature stabilization to 1°C can be easily achieved we

obtain $\tau_\ell < 9^\circ$ and $\frac{\sin \tau_\ell/2}{\tau_\ell/2} = 0.999$. So, even if this effect occurs only in one cavity it can still be neglected.

Another phase slip between particles and wave occurs at lower momenta because the particle velocity is appreciably different from $v_\varphi = c$. It is highest for protons at the lower limit of separation momenta (about 7 GeV/c).

Here we get $\tau_\ell/2 = 50^\circ$ giving

$$\frac{\sin \tau_\ell/2}{\tau_\ell/2} = 0.74$$

This is not negligible, but again it has no effect on the deflection cancellation of unwanted particles because it occurs in both cavities.

For 7 GeV/c $K^\pm$ we get already $\frac{\sin \tau_\ell/2}{\tau_\ell/2} = 0.99$

d) Errors due to aberrations in the cavities can be neglected and even if they would happen they are cancelled by the 1 : 1 lens system between RF 1 and RF 2.

e) Anisochronism due to lens aberrations and finite beam openings can be neglected in a two cavity separator, but in a three cavity separator with larger openings this should be studied in some detail.

f) Errors due to Finite Momentum Bite

As the phase difference τ_{ab} of two particles is proportional to $1/p^2$ (cf.(3)) we can put

$$\frac{\Delta \tau_{ab}}{\tau_{ab}} = -2 \frac{\Delta p}{p} \qquad (24)$$

thus relating the momentum bite to a phase shift fluctuation between the two unwanted particles.

Some of the tolerances obtained in the actual layout are listed in Table 3.

If the phase difference between two unwanted particles is exactly

$$\tau_{ab} = 2N\pi \qquad N = 1, 2, \ldots$$

we can always cancel the mean final deflection of the two unwanted particles but the beam is blown up by phase errors and field amplitude variations to $2(\delta + \Delta\delta)$ (2δ : beam divergence in the centre of RF 1). We only retain phase errors in the phasing system, phase errors due to finite momentum bite and errors due to field amplitude fluctuations, since all others are small enough to be neglected.

For the final deflection of particles a or b we get

$$\psi_{a,b}(t) = (\varphi + \Delta\varphi_1)\cos\omega t - (\varphi + \Delta\varphi_2)\cos(\omega t + \Delta\tau) \qquad (25)$$

$\Delta\varphi_1$, $\Delta\varphi_2$: errors of field amplitudes in RF 1 and RF 2.

$\Delta\tau$: total phase error; we put $\Delta\tau = \sqrt{\Delta\tau(\mathrm{Ph})^2 + \Delta\tau_{ab}^2}$ (26)

For the fluctuations in the amplitude of $\psi_{a,b}(t)$ we obtain [26] (to first order)

$$\Delta\psi_{a,b}^2 = (\Delta\varphi_1)^2 + (\Delta\varphi_2)^2 + (\varphi\,\Delta\tau)^2 \qquad (27)$$

We remember that the condition for best use of cavity acceptance is given by

$$\psi_w = 2\delta$$

If the phase slip between the unwanted and wanted particles is τ_{aw} and the phase slip between the wanted particle and the deflecting wave is τ_ℓ we get

$$\psi_w = 2\varphi \sin\frac{\tau_{aw}}{2} \cdot \frac{\sin\tau_\ell/2}{\tau_\ell/2} = 2\delta \qquad (28)$$

The relative increase in beam-stopper thickness needed to stop all particles a and b is then given by

$$\frac{\Delta\delta}{\delta} = \frac{\Delta\psi_{a,b}}{\delta} = \frac{\Delta\psi_{a,b}}{\psi_w/2} \qquad (29)$$

$$= \left[\sin\frac{\tau_{aw}}{2} \cdot \frac{\sin\tau_\ell/2}{\tau_\ell/2}\right]^{-1} \cdot \sqrt{\left(\frac{\Delta\varphi_1}{\varphi}\right)^2 + \left(\frac{\Delta\varphi_2}{\varphi}\right)^2 + (\Delta\tau)^2}$$

The necessary increase in beam-stopper thickness can be very big if the condition $\tau_{ab} = 2N\pi$ is not exactly fulfilled because the mean final deflection of only one kind of particle, say a, can be made zero. For the other one b, we get for the maximum final deflection

$$\psi_b = 2\varphi \sin\frac{\tau_{ab}}{2} \neq 0$$

this has to be added to $\Delta\psi_{a,b}$ and we get now for the relative increase in beam-stopper thickness

$$\frac{\Delta\delta}{\delta} = \left(\sin\frac{\tau_{aw}}{2} \cdot \frac{\sin\tau_\ell/2}{\tau_\ell/2}\right)^{-1} \left[2\sin\frac{\tau_{ab}}{2} + \sqrt{\left(\frac{\Delta\varphi_1}{\varphi}\right)^2 + \left(\frac{\Delta\varphi_2}{\varphi}\right)^2 + (\Delta\tau)^2}\right] \qquad (30)$$

For design momentum the factor in front of the square bracket equals 1.

The maximum errors on $\Delta\varphi_1$, $\Delta\varphi_2$ $\Delta\tau(Ph)$ are fixed by the actual layout of the separator and are listed in Table 3. $\Delta\tau_{ab}$ is fixed by the momentum bite accepted by the beam because

$$\Delta\tau_{ab} / \tau_{ab} = -2\ \Delta p/p$$

From (30) one can however deduce that $\frac{\Delta\delta}{\delta}$ is much more affected by the values of τ_{ab} than by the errors $\Delta\varphi$, $\Delta\tau$. This shows clearly the importance of the condition (4a)

$$\tau_{ab} = 2N\pi$$

in the case of two particle rejection.

We now calculate for a given $\frac{\Delta\delta}{\delta}$ the percentage η_{BS} of wanted particles that pass the beam-stopper.

First we remember that the deflection of the wanted particles behind RF 2 is modulated as $\sin\omega t$ and has a maximum value given by

$$\psi_w = 2\varphi \sin\frac{\tau_{aw}}{2}$$

We assume uniform distribution of the particles in the beam and $\psi_w \leq 2\delta$, the optimum condition being given by $\psi_w = 2\delta$

If the beam-stopper width corresponds to a half opening of the unwanted particle beam $\delta + \Delta\delta$ we get for the percentage of wanted particles passing the beam-stopper (cf. Fig.11)

$$\eta_{BS} = \frac{1}{2\pi\delta}\int_{\delta + \Delta\delta - \psi_w}^{\delta}\left(\pi - 2\ \text{arc sin}\ \frac{\delta + \Delta\delta - x'}{\psi}\right)dx'$$

$$= \frac{\Delta\delta}{\delta}\left[\frac{1}{\pi}\ \text{arc sin}\ \frac{\Delta\delta}{\psi_w} - 0.5\right] + \frac{\psi_w}{\pi\delta}\sqrt{1 - \left(\frac{\Delta\delta}{\psi_w}\right)^2} \qquad (31)$$

and $\frac{\Delta\delta}{\psi_w} \leq 0.25$ one can put in good approximation

$$\eta_{BS} = \frac{\psi_w}{\pi\delta} - 0.5\ \frac{\Delta\delta}{\delta} \qquad (31a)$$

For non-uniform distribution, e.g. triangular distribution of particles in the beam one gets values for η_{BS} smaller by some percent.

Under optimum conditions $\psi_w = 2\delta$, $\Delta\delta = 0$ one gets

$$\eta_{BS} = \frac{2}{\pi} \approx 64\ \%$$

In Table 4 we have listed values of $\Delta\delta/\delta$ and η_{BS} for some separation cases and two different values of momentum bite $\Delta p/p$. We take into account the tolerances given above and assume always $\psi_w = 2\delta$.

One notes the very low values of η_{BS} in the case of $\bar{p}$ separation at 18 - 20 GeV/c. They are due mainly to the values of $\tau_{ab} = {}_{\pi K}$ being widely

different from $2N\pi$ (cf. Table 1b)

One concludes from Table 4 that in the actual layout, best separation of antiprotons at 18 - 20 GeV/c is obtained for a flight path of 22 - 28 m.

Acknowledgements

It is a pleasure for me to thank cordially my colleagues from AR-Division Peter Bramham, Ron Fortune and Bryan Montague, for the close co-operation they have offered me during my stay in their group.

I would also like to thank the technicians involved in the construction and running of the RF-Separator.

Table 3

TOLERANCES OF ACTUAL LAYOUT

$\Delta f/f$	3.10^{-6}
$\Delta\tau(Ph)$	$\pm 3^{\circ}$
$\Delta\varphi_1/\varphi = \Delta\varphi_2/\varphi$	$\pm 2.5\%$
ΔT	1° C.

Table 4

Values of $\Delta\delta/\delta$ and η_{BS}

Length m.	Momentum GeV/c.	Particle	$\Delta p/p$ %	$\Delta\delta/\delta$	η_{BS} %
50	10	$K^{\pm}$	$\pm$ 0.25	0.14	57
			$\pm$ 0.50	0.26	51
	14	$K^{\pm}$	$\pm$ 0.25	0.12	58
			$\pm$ 0.50	0.19	54
50	18	$\bar{P}$	$\pm$ 0.25	1.17	17
			$\pm$ 0.50	1.17	17
	20	$\bar{P}$	$\pm$ 0.25	0.86	26
			$\pm$ 0.50	0.87	26
28	18	$\bar{P}$	$\pm$ 0.25	0.67	34
			$\pm$ 0.50	0.67	34
	20	$\bar{P}$	$\pm$ 0.25	0.71	32
			$\pm$ 0.50	0.71	32
22	20	$\bar{P}$	$\pm$ 0.25	0.65	35
			$\pm$ 0.50	0.65	35

APPENDIX I

Definitions and relations for electromagnetic fields in waveguides

We introduce:

P_o	: input power
I	: voltage attenuation coefficient
E	: electrical field
z	: coordinate of the axial direction
v_g	: group velocity of a wave
v_φ	: phase velocity of a wave
λ	: free space wavelength
λ_g	: wavelength in the guide
$f = \frac{\omega}{2\pi}$	: frequency

for a waveguide with losses we get $E(z) = E_o\, e^{-Iz}$ (1a)

and $P(z) = P_o\, e^{-2Iz}$ (1b)

The definition of shunt impedance (resistance per unit length) is

$$r = \frac{(\text{electrical field})^2}{\text{power lost/unit length}} \quad \frac{\Omega}{m}$$

For a linear accelerator structure this is proportional to

$$\frac{(\text{energy gained/unit length})^2}{\text{power lost per unit length}}$$

and is one of the figures of merit of a waveguide because it gives the efficiency of a waveguide for transmitting energy to a particle.

An analogous quantity can be defined for a deflecting waveguide.

The deflecting force on a particle in synchronism with a wave is given by [8]

$$F_T = \frac{e}{k}\, \text{grad}_T\, E_z \qquad (2)$$

e : charge, $k : \frac{2\pi}{\lambda}$

for a wave that is linearly polarised in x-direction we get

$$F(x) = \frac{e}{k}\, \frac{\partial E_z}{\partial x} \qquad (2a)$$

now we can define a transverse shunt impedance r_T by

$$r_T(x) = \frac{\left[\frac{1}{k}\, \frac{\partial E_z}{\partial x}\right]^2}{-\, dP/dz} \qquad (3)$$

from (1b) we get $\frac{dP}{dz} = -2I\,P(z)$ (4)

thus $$r_T(x) = \frac{\frac{1}{k}\frac{\partial E_z}{\partial x}^2}{2I\,P(z)} \quad (3a)$$

The stored energy/unit length $w(z)$ is related to the power by

$$P(z) = w(z)\,v_g \quad (5)$$

assuming that the group velocity v_g is equal to the velocity of energy transport.

The quality factor of a waveguide is defined

$$Q = \frac{2\pi \text{ energy stored/unit length}}{\text{energy dissipated/unit length per cycle}}$$

with (4) and (5) we get

$$Q = \frac{2\pi\,w(z)}{\frac{dP}{dz}\cdot\frac{1}{f}} = \frac{\omega}{2I\,v_g} \quad (6)$$

Combining (3a) and (6) we get

$$\frac{r_T}{Q} = \frac{\left[\frac{1}{k}\frac{\partial E_z}{\partial x}\right]^2}{P(z).\omega}\cdot v_g \quad (7)$$

as $\left.\frac{\partial E_z}{\partial x}\right|_z = \left.\frac{\partial E_z}{\partial x}\right|_{z=0}\cdot e^{-Iz}$, and as $P(z) \alpha E_z^2$, this quantity is independent of losses and only dependent on the geometry of the waveguide.

(7) can be written for z = 0

$$\left[\frac{1}{k}\left.\frac{\partial E_z}{\partial x}\right|_o\right]^2 = P_o\cdot\frac{1}{v_g}\cdot\frac{r_T}{Q}\,\omega \quad (7a)$$

and shows: for a given input power P_o the deflection force increases with decreasing v_g.

The filling time of a waveguide of length ℓ supporting a travelling wave with group velocity v_g is given by

$$t_f = \frac{\ell}{v_g} \quad (8)$$

thus combining (7a) and (8) we can state also that for given input power P_o the deflection force increases with filling time.

t_f affects the dimensional and frequancy tolerances of a structure. This can be seen by introducing the dispersion D of a waveguide.

We define $D = \frac{c}{v_g} - 1 = \frac{c.t_f}{\ell} - 1$

and use the definition $v_g = \frac{\partial k_g}{\partial k}$ (9)

$\left(k = \frac{2\pi}{\lambda}\ ;\ k_g = \frac{2\pi}{\lambda_g}\right)$

one gets easily for $v_\varphi = c$

$$D \frac{\Delta f}{f} = - \frac{\Delta v_\varphi}{v_\varphi} = \frac{\Delta \lambda_g}{\lambda_g} \qquad (10)$$

thus, in a waveguide with dispersion D changes of v_φ with frequency are D times higher than in free space.

The same applies to dimensional changes $\Delta r/r$ caused by temperature changes which can be related to changes in frequency by

$$\frac{\Delta r}{r} = - \frac{\Delta f}{f} \qquad (11)$$

Finally we can get the change in phase ϕ due to a change in frequency by using the relation

$$\frac{\Delta \phi}{2\pi} = \frac{\Delta \lambda_g}{\lambda_g} .n \qquad (12)$$

where n is the number of wavelength corresponding to ℓ.

Combining (9) and (10) one gets

$$\Delta\phi = 2\pi.D \frac{\Delta f}{f} \ n \qquad (12a)$$

indicating that a phase change is also directly proportional to D and thus depending on the filling time.

A more detailed discussion of these relations can be found in a paper of Montague.[27]

APPENDIX II

Choice of Waveguide dimensions

We discuss briefly the choice of the waveguide dimensions finally adopted and some of its properties. (notation from Appendix I)

Adjustable parameters of the waveguide (cf. Fig. 3) are a, b, d and D (which corresponds to the number of cells per wavelength) and the length ℓ. They are closely related to some characteristic quantities of the waveguide like phase and group velocity v_φ and v_g, filling time t_f, voltage attenuation coefficient I and Q-value (cf. also [28]).

We recall that the frequency was chosen around 2855 MHz. This fixes approximately the radius b of the disc-loaded waveguide which must be nearly equal to the cut-off radius of an unloaded (smooth) waveguide.

One of the most important conditions being $v_\varphi = c$ the first computations were all done under this assumption.

A basic quantity of a structure is the filling time t_f given by $t_f = \frac{\ell}{v_g}$.

As for a given input power, the deflection force is proportional to the filling time (cf. Appendix I, 7a), t_f should be long. However, for long t_f, dimensional and frequency tolerances necessary for the high phase stability needed in a RF-Separator become very tight and put an upper limit on t_f which lies around 0.5 μsec.

For the determination of ℓ we note that the deflection angle of wanted particles is given by

$$\psi_w = \frac{2eE}{pc} \sin \frac{\tau_{aw}}{2} \qquad \text{(cf. (18))}$$

As we are limited in input power (and thus in the deflection field strength $\bar{E}$) to about 10 - 20 MW, and as the deflection angles should be around 1 mrad at p = 10 - 20 GeV/c, (18) fixes a lower limit for ℓ.

The final choice was $\ell = 3$ m.

Once t_f and ℓ are fixed we have also fixed $\frac{v_g}{c} \approx \frac{1}{50}$

One knows that the value of v_g is mainly dependent on the coupling between the different cells of the waveguide, thus the choice of v_g fixes to a large extent the value of the inner radius a. It is still slightly affected by the sign of v_g being somewhat higher for positive v_g.

The final choice was done by computing $v_g(a)$ for different values of the cell pitch D (number of cells per wavelength) and the disc thickness d. A positive v_g was chosen on the grounds of higher acceptance although the deflection force is somewhat smaller for the same input power. For the same reason the number of cells per wavelength were chosen to be 4 whilst the maximum for deflection force was around 3.

Finally, as can be seen from the relation

$$\omega t_f = 2I\,Q\,\ell \qquad \text{(cf. Appendix I, (6) and (8))}$$

I is fixed by the choice of t_f.

The parameters chosen are listed in Table 2 and Fig. 3. They are partly obtained by measurements[12] on models and actual waveguides made to guide and underly the computer studies. Fig. 12 shows the dispersion diagram[11] of the waveguides. The slope of the curves is proportional to the group velocity. One notes that the EH_{11} deflecting mode can only be excited in a narrow frequency band and that its wavelength (or phase shift per cell) is a complicated function of frequency. The phase shift per cell which is fixed by the number of cells per wavelength can range from 0 (for $\lambda_g = \infty$) to π (for $\lambda_g = 2D$), higher phase shifts being physically indistinguishable from a corresponding phase shift in this range.

The working frequency is given by the intersection of the curve with the line $v_\varphi = c$ (which passes through the origin of coordinates). At this frequency there are however two modes (with different guide wavelength) possible. The unwanted one is eliminated by correct design of the coupler[29] (mode transformer) between the rectangular waveguide feeding the RF power and the structure.

In Fig. 13 we have represented this coupler and a part of the waveguide with a sketch of the field configuration inside.

References

1) V.A. Vagin, V.I. Kotov, I.N. Semenyushkin, Sov.Phys. Uspekhi 7, 305 (1964) (Review-article)

2) M.M. Geiger, P. Lapostolle, B.W. Montague, CERN Report 61-26

3) M. Bell, P. Bramham, R.D. Fortune, E. Keil, B.W. Montague, Intern.Conf. on High Energy Accelerators, Dubna 1963, 798

4) P. Bramham, R.D. Fortune, E. Keil, H. Langeler, B.W. Montague, W.W. Neale, Phys. Letters 15, 290 (1965)

5) D. Dekkers et al. Phys. Rev. 137, B962 (1965)

6) O_2-beam : E. Keil, W.W. Neale, Int.Conf. on High Energy Accelerators, Dubna, 1963, 782
E. Keil, AR/Int. PSep/63-6 (1963)
U_1-beam : P. Lazeyras, private communication.

7) W. Schnell, CERN Report 61-5

8) Y. Garault, CERN Report 64-43

9) B.W. Montague, to be published

10) M. Bell, P. Bramham, B.W. Montague, Nature 198, 277 (1963)

11) P. Bramham, AR/Int. PSep/63-4

12) H. Hahn, Rev.Scient.Instr. 34, 1094 (1963)
H. Hahn, BNL Internal report AGS HH.4 and HH.5 (1962)
H. Hahn, H.J. Halama, BNL Acc.Dept. Internal report HH/HJH.2 (1963)

13) H.G. Hereward, M. Bell, CERN Report 63-33

14) H.G. Hereward, M. Bell, to be published.

15) B.W. Montague, CERN PS/Int. AR/PSep/60-1

16) B.W. Montague, AR/Int. PSep/65-3 (to be presented to the Frascati Conf. on High Energy Accelerators 1965)

17) B.W. Montague, AR/Int. PSep/63-1

18) P.B. Wilson, Nucl. Instr. and Methods, 20, 336 (1963)

19) H.A. Schwettman, P.B. Wilson, J.M. Pierce, Fairbank HEPL - 349 (1964)

20) E. Keil, AR/Int. PSep/62-3

21) P. Bramham, AR/Int. PSep/65-2

22) R. Fortune, AR/Int. PSep/65-4 ; P. Bramham, AR/Int. PSep/65-5.

23) P. Bramham, CERN Report 65-9
CERN Report in preparation

24) P. Rotelli, to be published.
J. Delfosse, private communication

25) R. Fortune, AR/Int. PSep/65-6.

26) E. Keil, AR/Int. PSep/63-3

27) B.W. Montague, to be published.

28) O.A. Altenmueller, R.R. Larsen, G.A. Loew, SLAC - 17 (1963)

28) P. Bramham, M.J.G. Lee, CERN Report 64-14

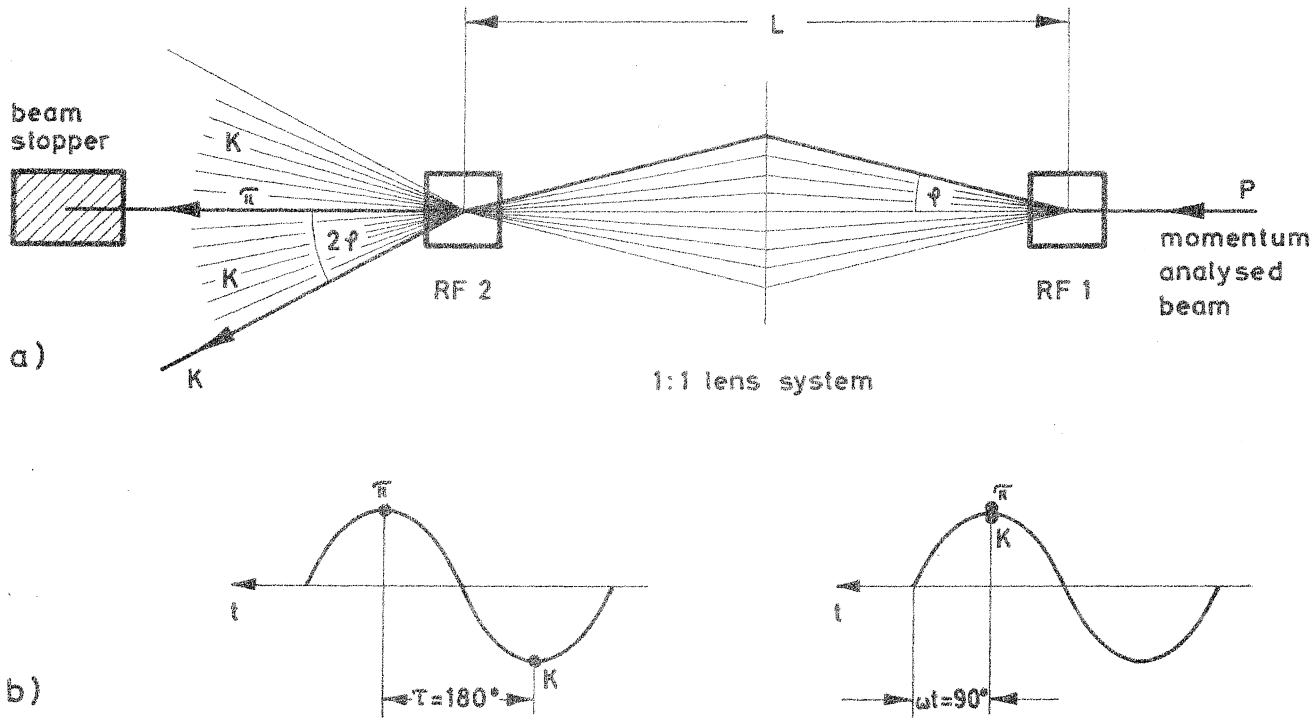

Fig. 1a: Principles of operation of RF-Separator

1b: Phase relations of two particles of different rest-mass with respect to travelling wave

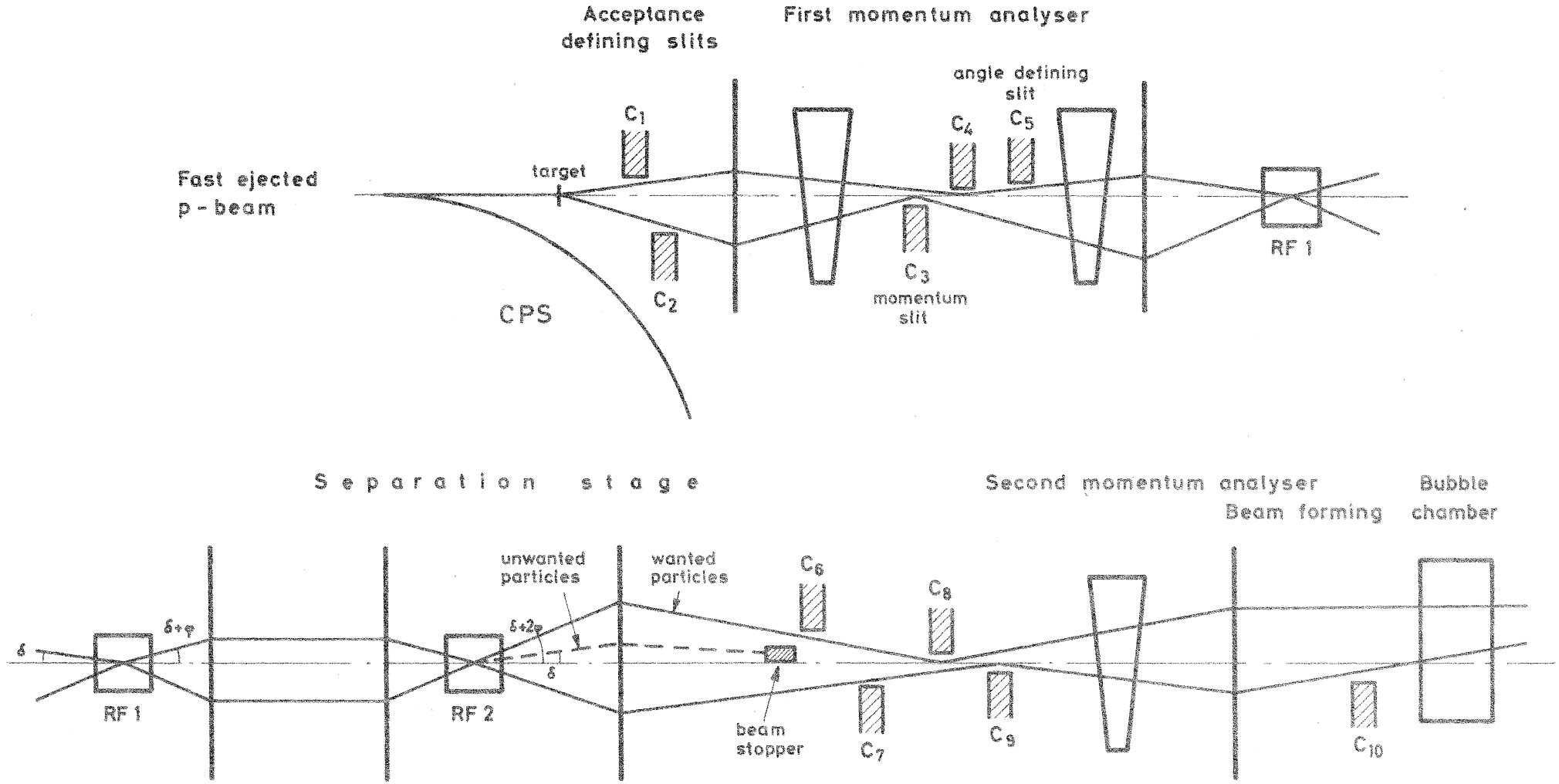

Fig. 2: Schematic layout of a RF - separated beam

above centre line: vertical (mass - separation) plane

under centre line: horizontal (momentum analysis) plane

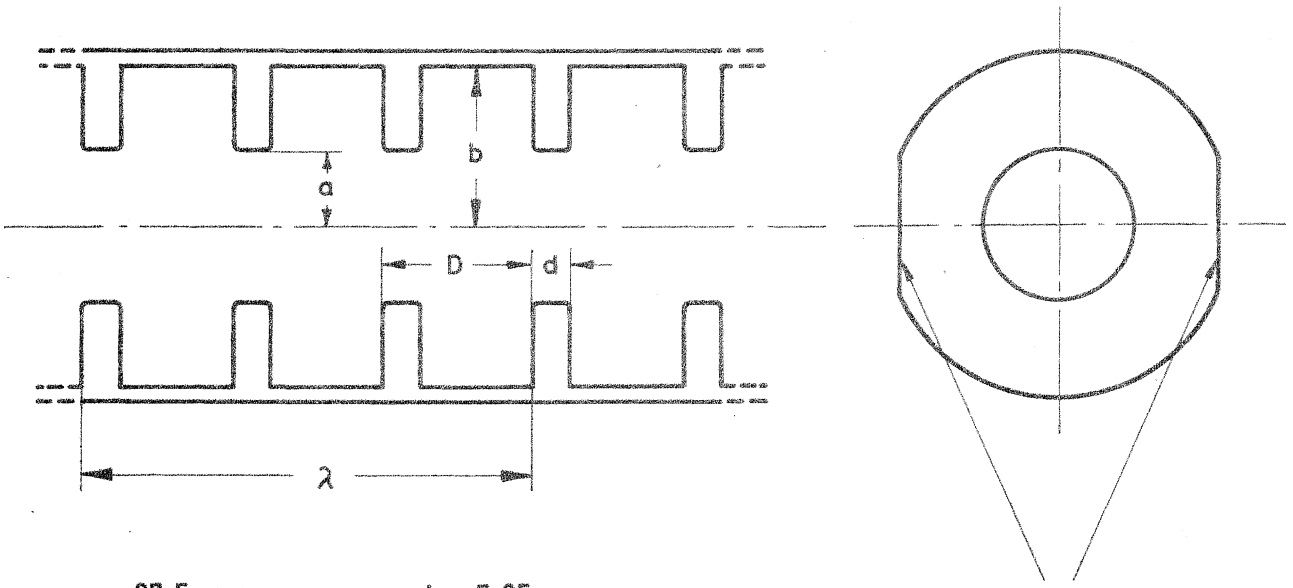

a = 27.5 mm
b = 57.8 mm

d = 5.25 mm
D = 26.25 mm

f = 2855 MHz

λ = 10.5 cm

Fig. 3 : Iris-loaded waveguide

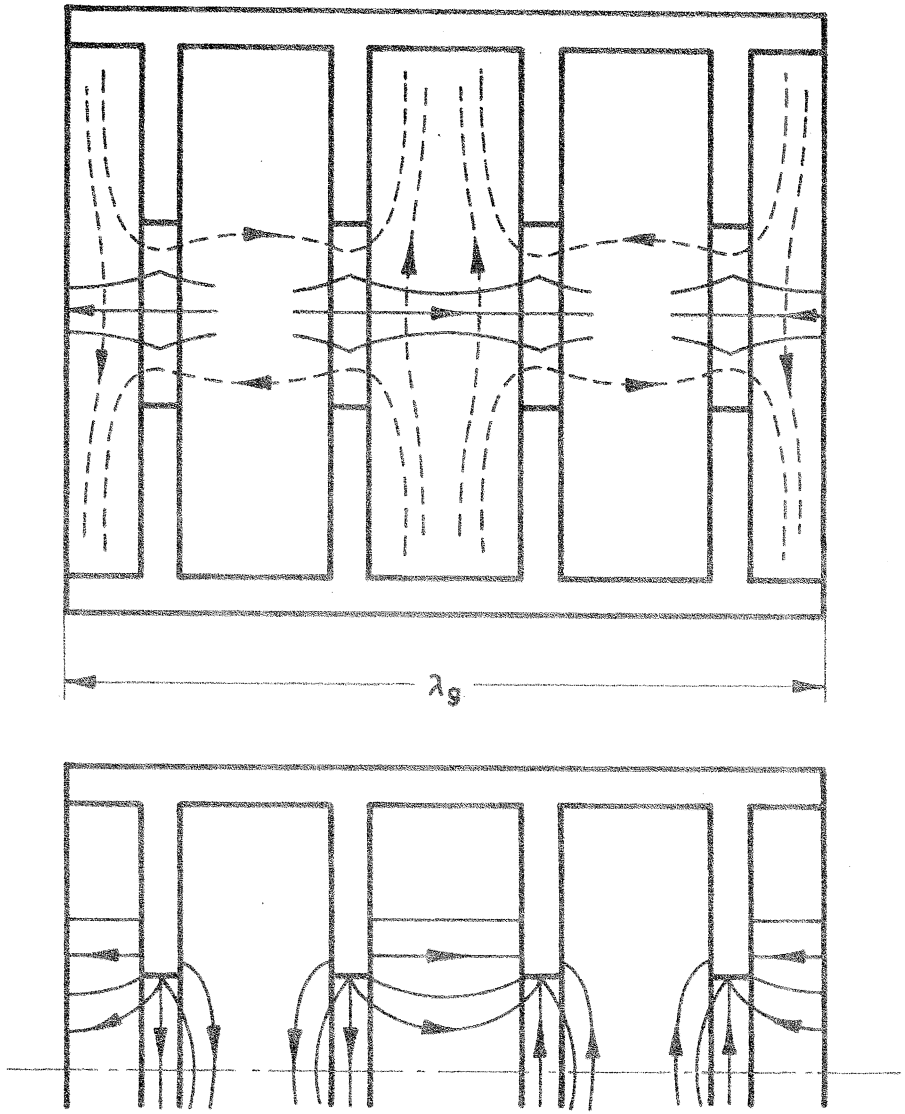

Fig. 4 :
Field-lines inside the loaded waveguide
hybrid deflecting mode $(EH)_{11}$
phase shift per cell : $\pi/2$

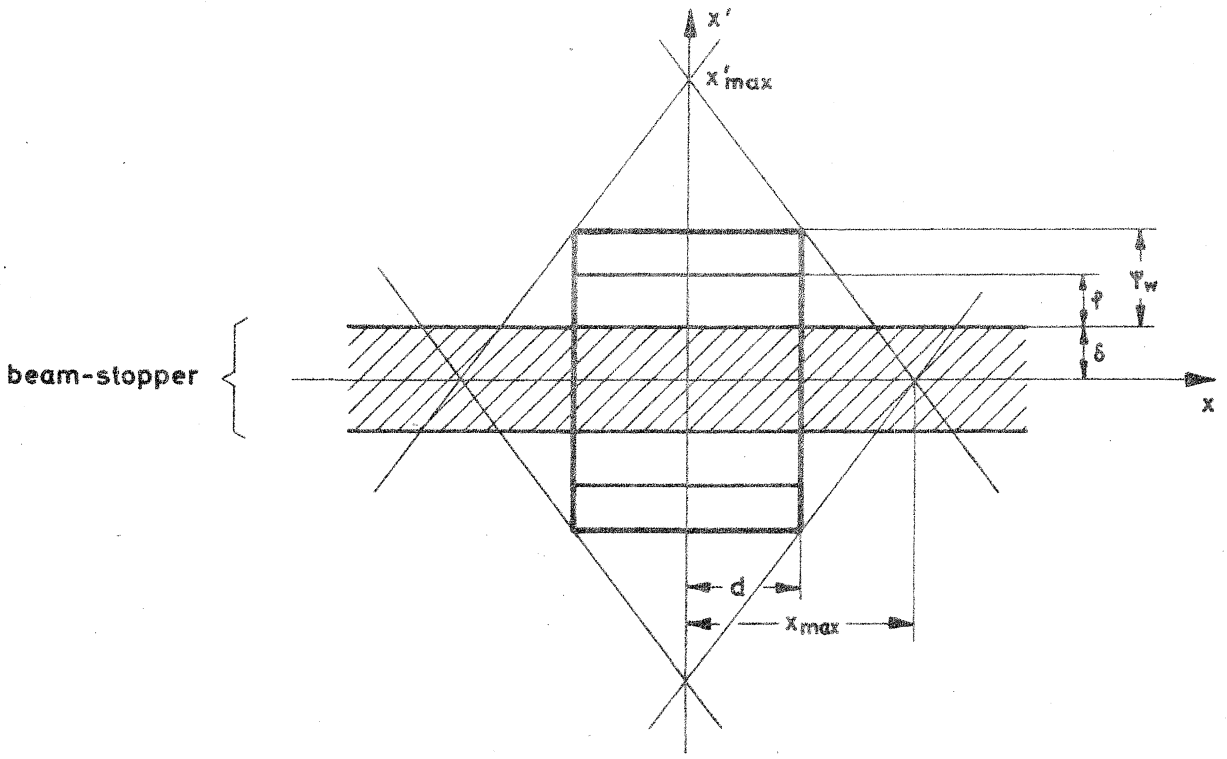

Fig. 5 : Phase plane diagram for the center of the first cavity

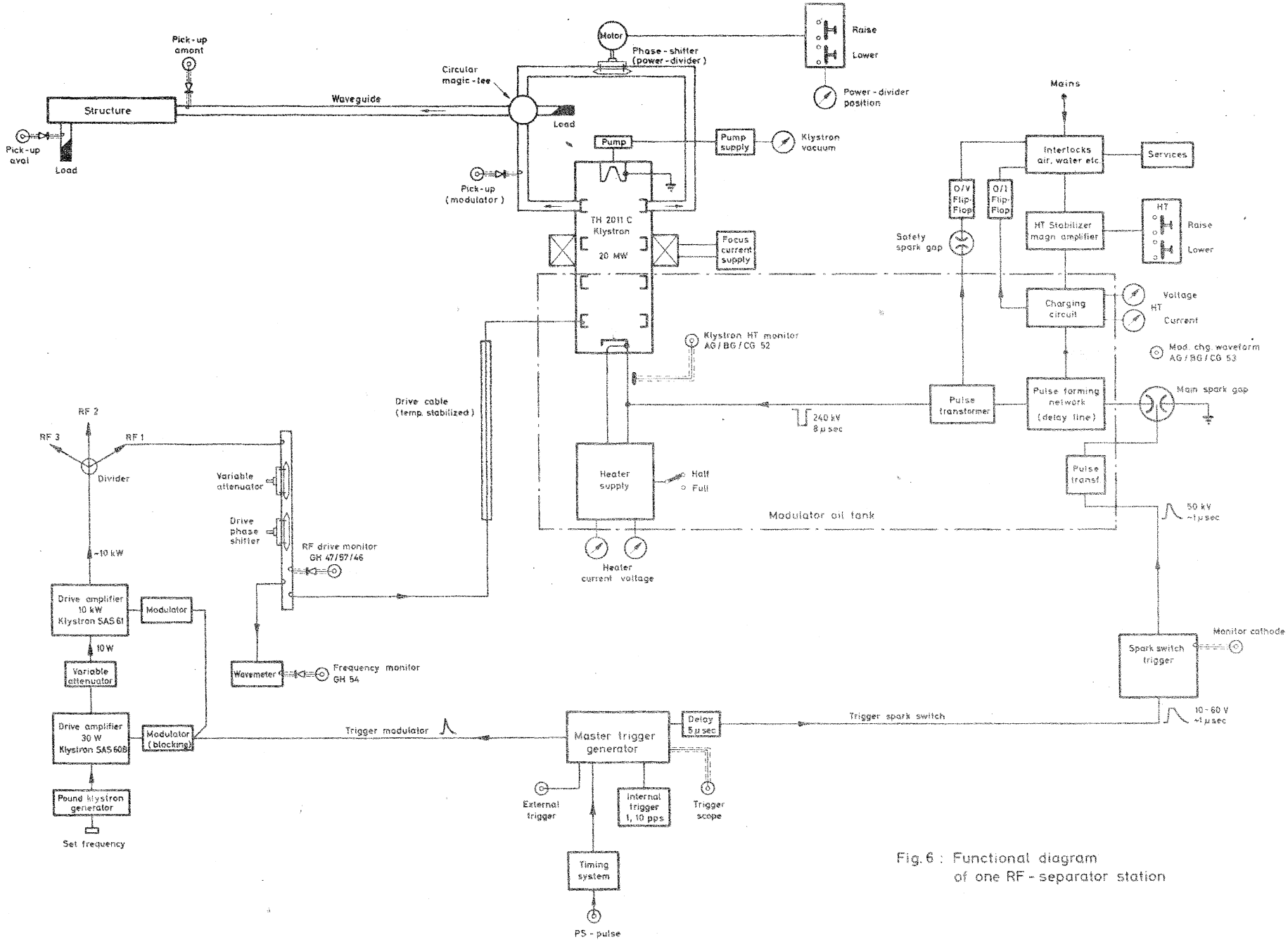

Fig. 6 : Functional diagram of one RF - separator station

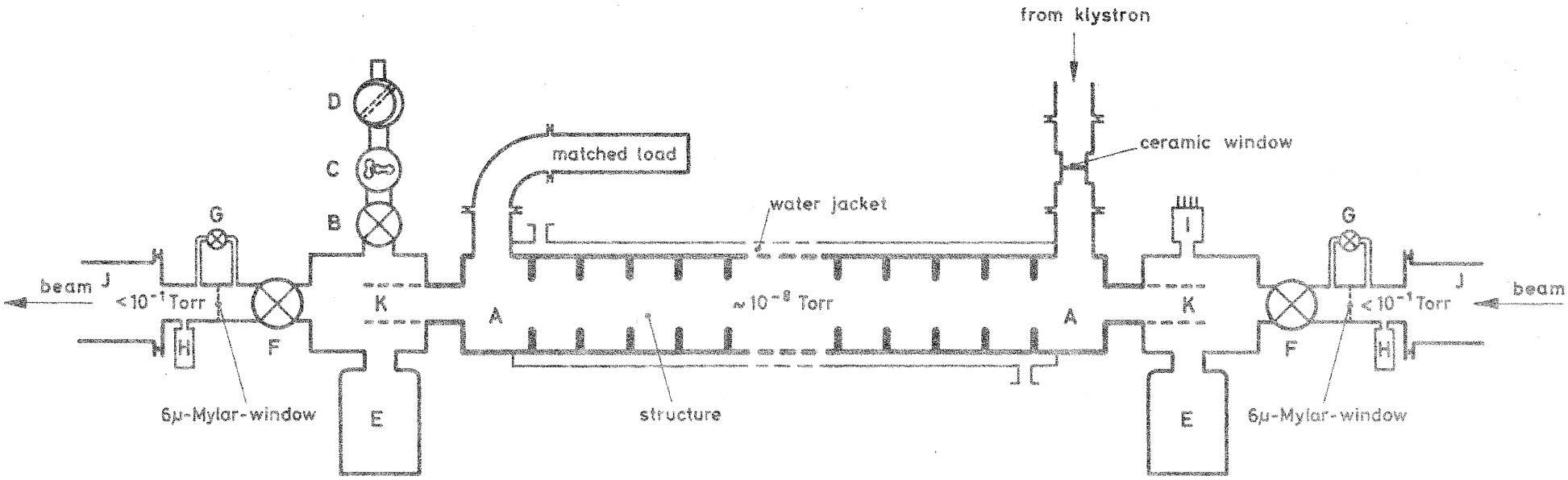

A Coupler
B High vacuum valve
C Roots pump
D Rotary pump
E Titanium-pump
F 90°-high vacuum valve
G By-pass for Mylar-window
H Thermocouple
I Ionisation Gauge
J Beam-tube
K Cylinder to prevent leaking out of RF

Fig. 7 : Structure vacuum system

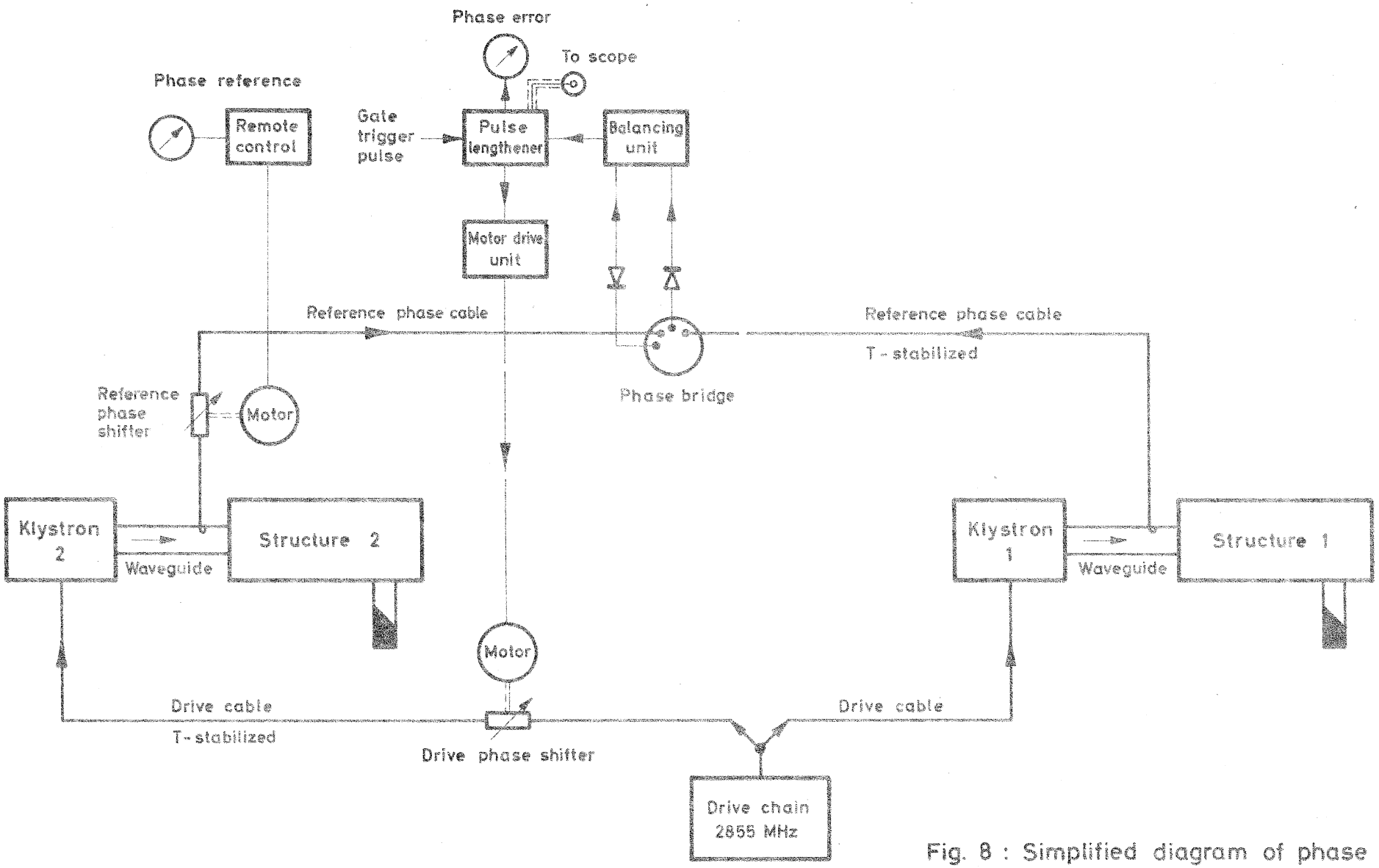

Fig. 8 : Simplified diagram of phase servo for RF-separator

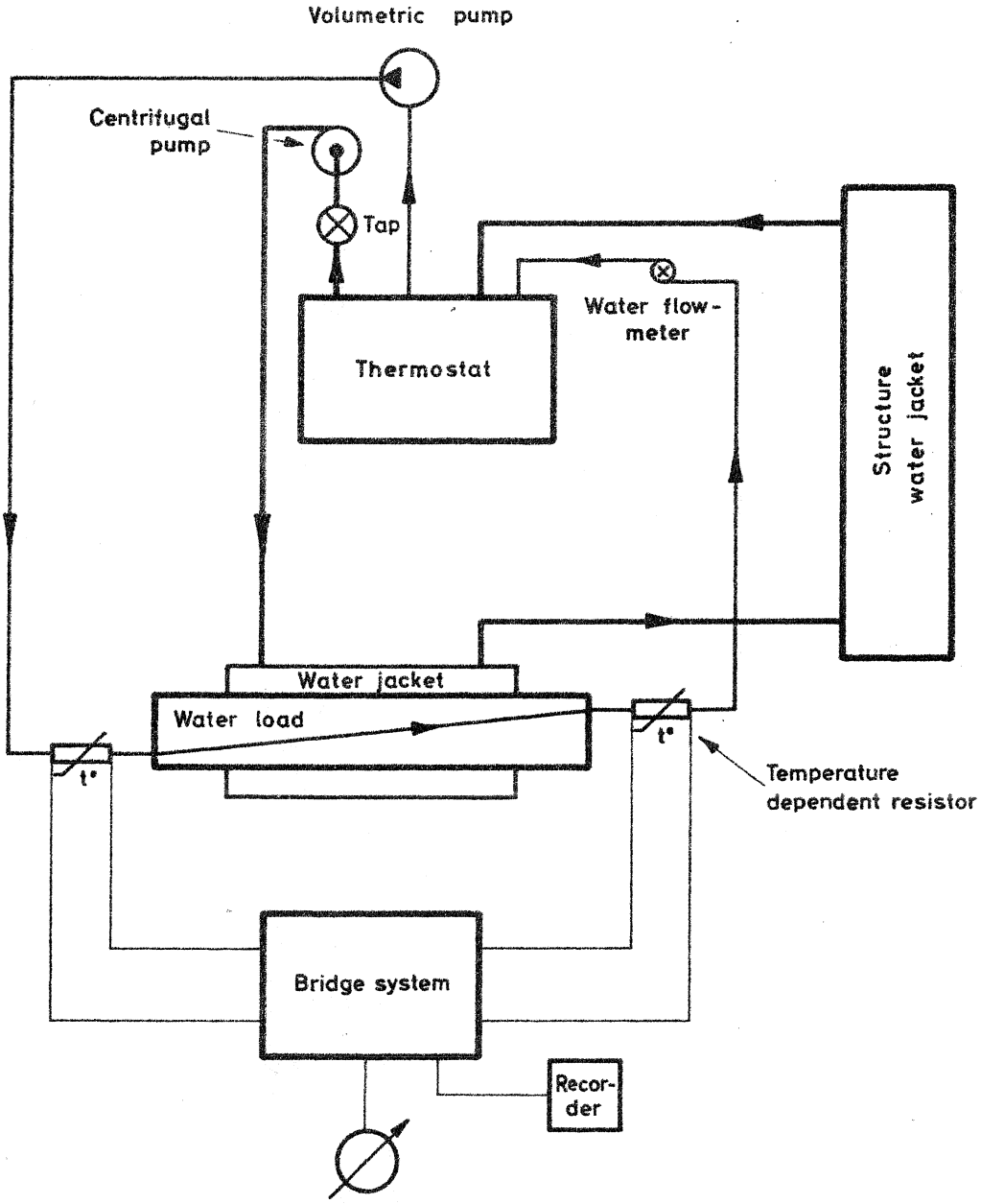

Fig. 9 : Layout of water cooling system and power measurement system

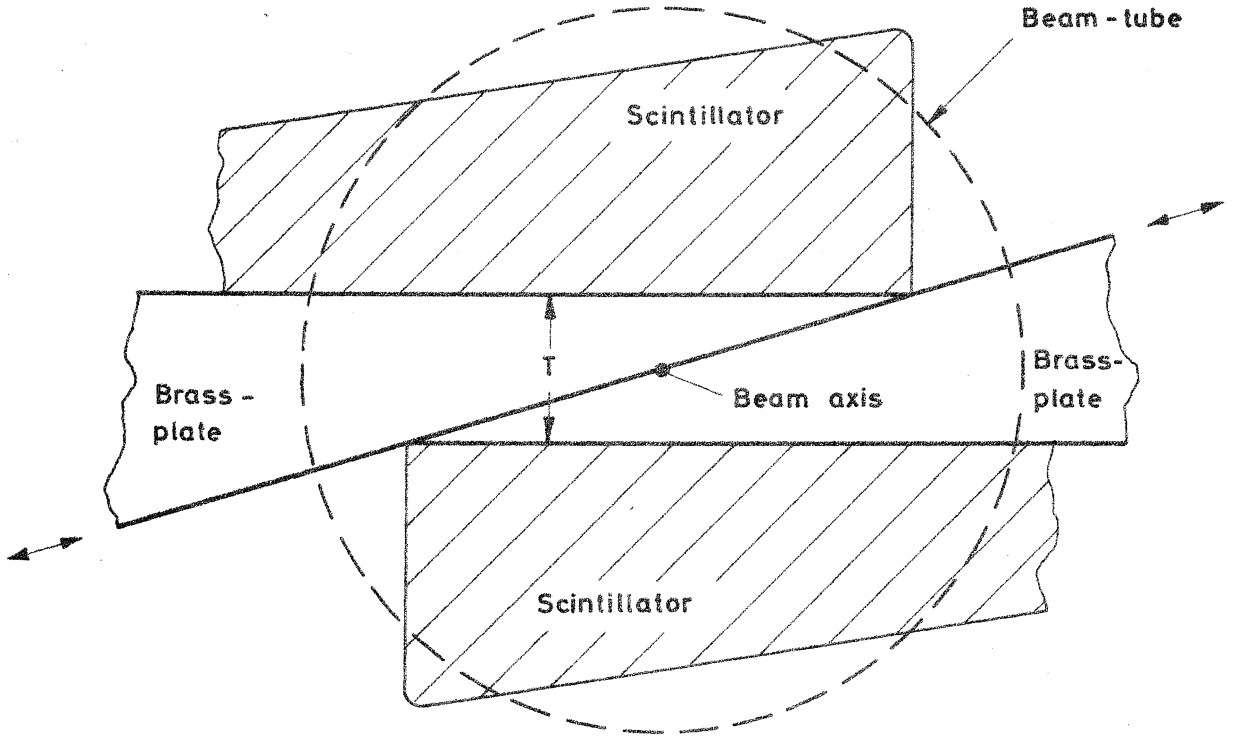

Fig. 10 : Beam - stopper

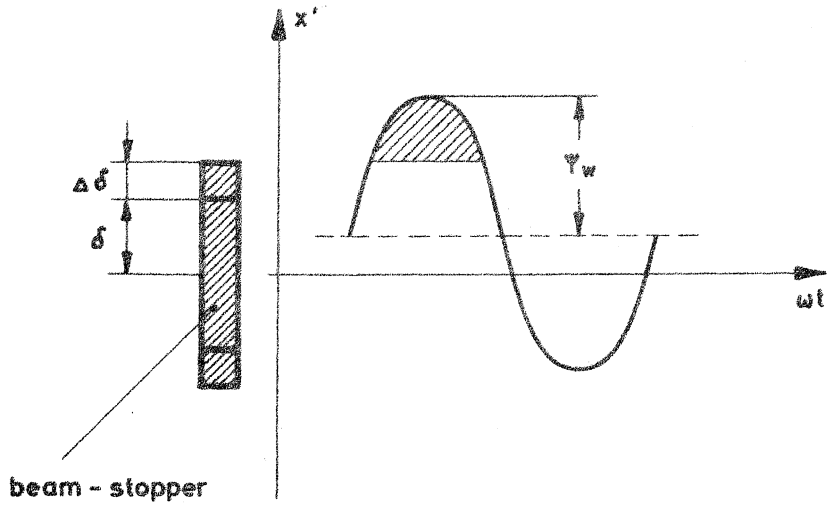

Fig. 11

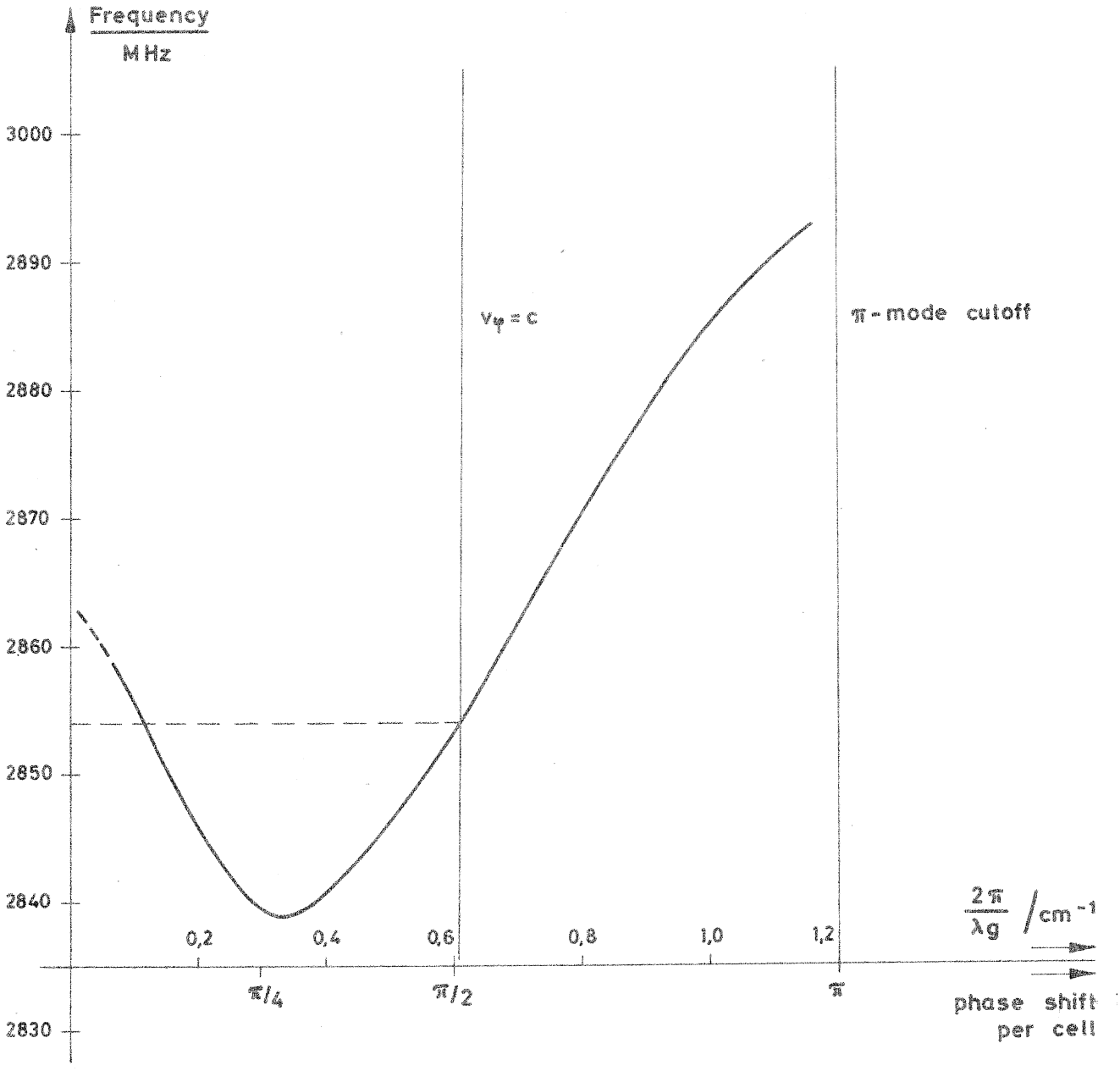

Fig. 12 :

Measured Brillouin (dispersion) diagram for $(EH)_{11}$ deflecting mode
(in air)

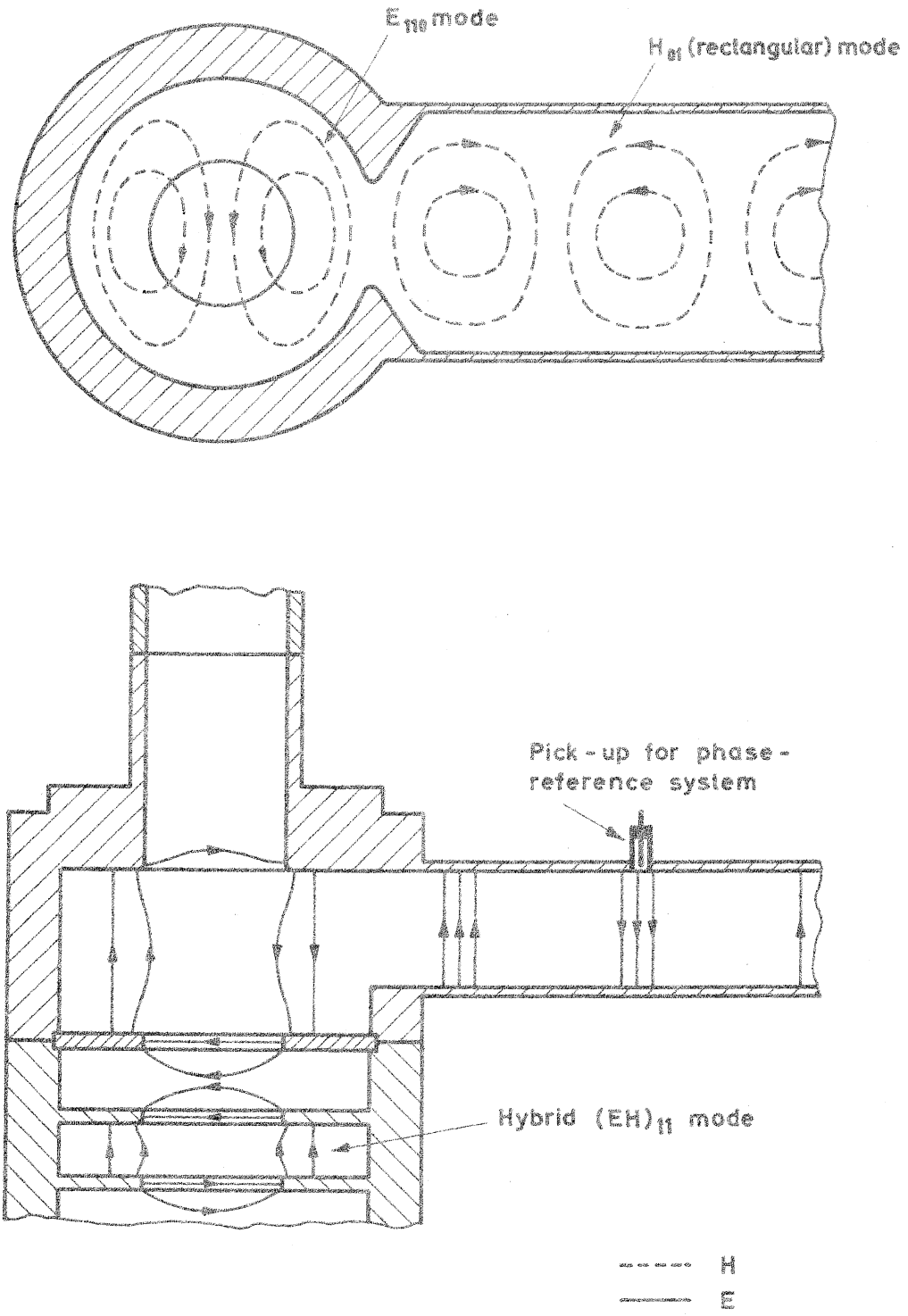

Fig. 13 : Mode transformation in the coupler